

October 2008

Dynamics of a nonlinear microresonator based on resonantly interacting flexural-torsional modes

Ashwin Vyas

Purdue University, ashwinv@purdue.edu

Dimitrios Peroulis

Birck Nanotechnology Center and School of Electrical and Computer Engineering, Purdue University, dperouli@purdue.edu

Anil Bajaj

Purdue University, anil.k.bajaj.1@purdue.edu

Follow this and additional works at: <http://docs.lib.purdue.edu/nanopub>

Vyas, Ashwin; Peroulis, Dimitrios; and Bajaj, Anil, "Dynamics of a nonlinear microresonator based on resonantly interacting flexural-torsional modes" (2008). *Birck and NCN Publications*. Paper 123.

<http://docs.lib.purdue.edu/nanopub/123>

This document has been made available through Purdue e-Pubs, a service of the Purdue University Libraries. Please contact epubs@purdue.edu for additional information.

Dynamics of a nonlinear microresonator based on resonantly interacting flexural-torsional modes

Ashwin Vyas · Dimitrios Peroulis · Anil K. Bajaj

Received: 2 November 2006 / Accepted: 21 December 2007 / Published online: 22 January 2008
© Springer Science+Business Media B.V. 2008

Abstract A novel microresonator operating on the principle of nonlinear modal interactions due to autoparametric 1:2 internal resonance is introduced. Specifically, an electrostatically actuated pedal-microresonator design, utilizing internal resonance between an out-of-plane torsional mode and a flexural in-plane vibrating mode is considered. The two modes have their natural frequencies in 1:2 ratio, and the design ensures that the higher frequency flexural mode excites the lower frequency torsional mode in an autoparametric way. A Lagrangian formulation is used to develop the dynamic model of the system. The dynamics of the system is modeled by a two degrees of freedom reduced-order model that retains the essential quadratic inertial nonlinearities coupling the two modes. Retention of higher-order model for electrostatic forces allows for the study of static equilibrium positions and static pull-in phenomenon as a function

of the bias voltages. Then for the case when the higher frequency flexural mode is resonantly actuated by a harmonically varying AC voltage, a comprehensive study of the response of the microresonator is presented and the effects of damping, and mass and structural perturbations from nominal design specifications are considered. Results show that for excitation levels above a threshold, the torsional mode is activated and it oscillates at half the frequency of excitation. This unique feature of the microresonator makes it an excellent candidate for a filter as well as a mixer in RF MEMS devices.

Keywords Microelectromechanical resonators · Parametric resonance · Autoparametric resonance · Internal resonance · Flexural-torsional oscillations

1 Introduction

Resonantly actuated micro-structures, referred to as microresonators, are an integral part of many MEMS devices such as highly sensitive pressure sensors, mass sensors [1], biological sensors [2], scanning force and atomic force microscopes, and radio frequency (RF) filters [3]. Geometric and inertial nonlinearities due to structure as well as the nonlinearities due to actuation mechanisms play important role in the dynamics of these microstructures. For example, in the AFM cantilever probes' resonant dynamics, van der Waals

A. Vyas · A.K. Bajaj (✉)
School of Mechanical Engineering, Purdue University,
585 Purdue Mall, West Lafayette, IN 47907-2088, USA
e-mail: bajaj@purdue.edu

A. Vyas
e-mail: ashwinv@purdue.edu

D. Peroulis
School of Electrical and Computer Engineering, Birck
Nanotechnology Center, Purdue University, 1205 West
State Street, West Lafayette, IN 47907-2057, USA
e-mail: dperouli@purdue.edu

interactions are shown to lead to a softening nonlinear response while the short range repulsive forces lead to an overall hardening response [4]. Younis and Nayfeh [5] in a recent study stressed the importance of accounting for nonlinearities in modeling microsystems. An inaccurate representation of the nonlinearities can lead to an erroneous prediction of the frequency response and eventually failure of design based on the erroneous simulations. Furthermore, microresonators based on parametric resonances [6] have finite amplitude oscillations due to nonlinearity resulting in detuning from resonance.

The main objective of this paper is to propose microresonators which depend in an essential way on nonlinear modal interactions between different modes for their functioning. In particular, the paper presents the concept, working principle, and modeling approach for a nonlinear pedal-type microresonator which is based on 1:2 internal resonance and modal interactions [7]. The pedal-type microresonator configuration has a flexural and a torsional mode of vibration. Though these modes are linearly uncoupled, the pedal structure exhibits inertial quadratic nonlinearities, and thus becomes a candidate for autoparametric 1:2 internal resonance between the two modes of the structure when the flexural and the torsional modes are designed to possess natural frequencies that are in a 2 to 1 ratio.

The motivation and guidance for this design came from such structures investigated on a macro scale. For example, Balachandran and Nayfeh [8] carefully modeled a L-beam structure and compared the simulation results with those of experiments with such a structure. The L-beam structure was designed to have 1:2 internal resonance between the first two modes of the structure. In such an internally resonant system, the directly excited mode at higher frequency, f , in turn excites a lower frequency mode with frequency $f/2$ due to quadratic nonlinear coupling between the two modes. This phenomenon, referred to as nonlinear modal interaction [7], can result in transference of much of the input or excitation energy from the higher frequency mode to the lower frequency mode, and was utilized for designing autoparametric vibration absorbers [9]. The attenuation of the higher mode response is accompanied by a large amplitude response of the lower mode. Thus, the lower mode acts like an autoparametric resonator. This nonlinear interaction with the accompanying high-amplitude response is exploited in

the present study to develop autoparametric MEMS mechanical resonators. Now, it is well known that the indirect response of the lower mode is due to parametric instability of the directly excited higher mode (pitchfork bifurcation) and this response exists only in the frequency range where actuation amplitude exceed some threshold actuation amplitude [10]. Thus, the response can be highly frequency selective, and the frequency selectivity can be controlled by the actuation amplitudes (e.g., actuation voltage for electrostatic actuation). Potential applications of such a frequency selective response of the indirectly excited mode include mass sensors, RF filters, sensitive pressure sensors, etc.

Apart from the pedal-type microresonator detailed in this paper, some plausible microstructure design configurations that also utilize autoparametric internal resonance are a micro L-beam structure, a micro T-beam structure, or a comb drive folded beam structure added with another beam mass structure. Essentially, the design needs to ensure that the two resonant modes are such that the movement of the higher mode results in parametric excitation of the lower mode. Vyas and Bajaj [11] recently presented a possible design and its nonlinear response for a T-beam microstructure that is excited electrostatically.

The modeling approach illustrated here provides a road map for modeling other possible designs as well. Electrostatic actuation is the most commonly used approach of exciting these structures, and is included in the model of pedal microresonator. Note that a linear model of this resonator will not be able to predict any interaction between the modes as the two modes are only coupled via nonlinear terms, with the lowest coupling nonlinear term being quadratic. Thus, a nonlinear continuum model of the resonator is presented via a Lagrangian formulation. In addition to the usual elastic strain energy and the kinetic energy of the structural elements, the model also retains electrostatic actuation nonlinearities which define the structure's equilibrium position. The linearized model is used to develop natural frequencies and mode shapes, and a two-mode reduced-order model is developed using the appropriate linear modes that are likely candidates for nonlinear interactions. The dependence of natural frequencies on bias voltages is formulated. Then the asymptotic method of averaging is used to determine amplitude equations that govern periodic response of the resonator about a static equilibrium position. The

resonator can either be excited directly in the first mode, or the second mode, by applying AC voltage to the appropriate electrodes. The performance of a typical nonlinear pedal microresonator to excitation of the higher frequency mode is explained by presenting analytical and simulation results for a structure designed to have internally resonant modes. The effects of damping, dimensional perturbations from nominal geometry needed for exact resonance, and perturbations in mass of the pedal on the resonator response are considered.

We should note here that microresonators based on parametric resonances, and those operating in torsional modes have been studied in the literature [1, 12]. The response of the system remains bounded due to the nonlinearities in the system, and specifically cubic nonlinearities play an important role [13]. The principal parametric resonance has been used in exciting nano [14] and micro [15] resonators oscillating in torsional mode by varying the stiffness of the resonator at twice the natural frequency. Zhang et al. [15] tuned the cubic nonlinearity in the torsional resonator by adjusting the actuation voltage and this tuning resulted in adjusting the bandwidth and selectivity of the resonator. Zhalutdinov et al. [16] used a low power laser to optically (thermally) excite a disk shaped microresonator. The temperature change due to laser heating results in change in stiffness and the temperature is modulated at twice the natural frequency to excite the microstructure parametrically in principal parametric resonance.

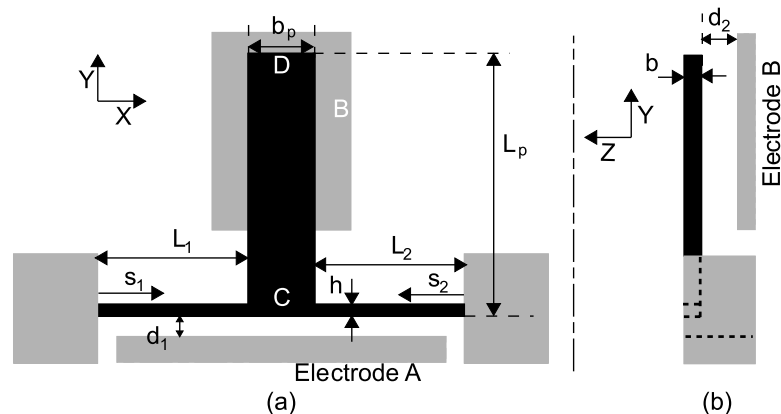
This work is organized as follows. A brief description of the system along with its operation principle is given in Sect. 2. Section 3 presents linear analysis for the pedal structure to determine design condi-

tions for 1:2 internal resonance of the first two modes. In Sect. 4, a two-mode approximate model is developed that determines the nonlinear response of the pedal structure under resonant excitation of the second mode. In Sect. 5, results regarding the static pull-in effects are presented, and Sect. 6 derives the slow-amplitude evolution equations governing the asymptotic response of the structure. In Sect. 7, representative results on the response of the pedal resonator are presented along with the effects of model parameters. The work ends in Sect. 8 with a summary and some concluding remarks.

2 Nonlinear pedal microresonator: nomenclature and Lagrangian

A schematic of a pedal microresonator working on the principle of nonlinear interaction of flexural-torsional modes is shown in Fig. 1. A plate type structure (the pedal CD) of length L_p and width b_p is supported by two beams 1 and 2 of lengths L_1 and L_2 , respectively. The structure has same thickness “ b ” for the beams and the pedal. The beams are assumed to have uniform rectangular cross-sections with beam lateral thickness h . The schematic also shows two stationary electrodes A and B, with the electrode A used in the model to electrostatically actuate the microresonator in XY plane. The spans of the electrode A on beams 1 and 2 are l_1 and l_2 , respectively. The gap between electrode A and the beams is denoted by d_1 , and the gap between the electrode B and the pedal is denoted by d_2 . The electrode B with span “ l_3 ” serves the purpose of a sensing electrode in the device and senses displacement in Z direction.

Fig. 1 A schematic diagram of the pedal microresonator showing (a) top view, and (b) side view. The stationary elements of the microresonator are shown in gray color



The essential mode of operation of the pedal structure as a nonlinear resonator is as follows: The electrode A excites the beams 1 and 2 in their resonant flexural mode in the XY plane when an AC voltage is applied. The pedal CD moves as a rigid body in the XY plane. There is another elastic mode of the structure which is dominated by the torsional motion of the beams about the X axis. In the torsional mode, the pedal moves angularly out of the XY plane in Z-direction. Linearly, the flexural in-plane motion and the torsional motion about the X-axis are uncoupled though they are nonlinearly coupled. When the flexural in-plane motion of the beams exceeds a threshold amplitude, the torsional mode of the structure gets excited due to transfer of energy from the flexural mode via a parametric excitation like term in the equation of

motion for the torsional mode. This transfer of energy is most efficient or effective when the torsional mode frequency is nearly half that of the flexural mode frequency. This process is described as nonlinear modal interaction [7] and is best studied by the analytical model of the structure developed in the following.

The arc lengths of the beams 1, 2, and the pedal CD are denoted by s_1 , s_2 , and s_3 , respectively. v_i and w_i are the flexural displacements of the i 'th beam in Y and Z direction, respectively. The torsional angular displacements θ_i about the X axis of the i 'th beam are also included in the model. v_i , w_i , and θ_i are all functions of the i 'th beam arc length s_i .

The kinetic energy, T , and the potential energy, U , of the resonator with aforementioned torsional and flexural displacements can be written as [17]:

$$\begin{aligned}
 T &= \sum_{i=1}^2 \left(\frac{1}{2} \int_0^{L_i} m_b (\dot{v}_i^2 + \dot{w}_i^2) ds_i + \frac{1}{24} \int_0^{L_i} m_b (b^2 + h^2) \dot{\theta}_i^2 ds_i \right) \\
 &\quad + \frac{1}{2} M_p \left(\dot{v}_1^2 + \dot{w}_1^2 + b_p \dot{v}_1 \dot{v}'_1 + \frac{b_p^2 + L_p^2}{3} \dot{v}_1'^2 + \frac{b_p^2}{3} \dot{w}_1'^2 + \frac{L_p^2}{3} \dot{\theta}_1'^2 \right. \\
 &\quad \left. + L_p \dot{w}_1 \dot{\theta}_1 + b_p \dot{w}_1 \dot{w}'_1 + \frac{1}{2} L_p b_p \dot{w}'_1 \dot{\theta}_1 - L_p \dot{v}_1 v'_1 \dot{v}'_1 \right. \\
 &\quad \left. - L_p \left(\dot{v}_1 + \frac{b_p}{2} \dot{v}'_1 \right) \theta_1 \dot{\theta}_1 + \frac{1}{2} L_p b_p \dot{v}'_1 w_1 \dot{w}'_1 \right. \\
 &\quad \left. + \frac{2}{3} L_p^2 (\dot{v}'_1 \dot{w}'_1 \theta_1 + \dot{v}'_1 w'_1 \dot{\theta}_1) \right) \Big|_{s_1=L_1}, \\
 U &= \sum_{i=1}^2 \left(\frac{1}{2} \int_0^{L_i} E (I_1 v_i''^2 + I_2 w_i''^2) ds_i + \frac{1}{2} \int_0^{L_i} GK \theta_i'^2 ds_i \right) \\
 &\quad + \frac{1}{8} \frac{Ebh}{L_1 + L_2} \left(\left(\sum_{i=1}^2 \int_0^{L_i} v_i'^2 ds_i \right)^2 + \left(\sum_{i=1}^2 \int_0^{L_i} w_i'^2 ds_i \right)^2 \right) \\
 &\quad + M_p g \left(w_1 + \frac{b_p}{2} w'_1 + \frac{L_p}{2} \theta_1 \right) \Big|_{s_1=L_1} \\
 &\quad - \frac{1}{2} \epsilon_0 b (V_{b1} + V_{ac} \cos \Omega t)^2 \left(\frac{b_p}{d_1 + (v_1|_{s_1=L})} + \sum_{i=1}^2 \int_{L_i-l_i}^{L_i} \frac{1}{d_1 + v_i} ds_i \right) \\
 &\quad - \frac{1}{2} \epsilon_0 b_p V_{b2}^2 \int_{L_p-l_3}^{L_p} \frac{1}{d_2 + (w_1 + s_3 \theta_1)|_{s_1=L_1}} ds_3,
 \end{aligned} \tag{1}$$

where $I_1 = bh^3/12$ and $I_2 = hb^3/12$. m_b is the beam mass per unit length, M_p is the mass of the pedal structure, E is Young's modulus, G is the modulus of

rigidity for each beam, K is the Saint Venant torsion constant for noncircular cross-section [18], and g is the acceleration due to gravity. A prime here denotes

derivative with respect to the appropriate arc length, and a dot denotes derivative with respect to time t . In writing the expressions for kinetic and potential energies, the following assumptions are made from theory of slender beams [17, 19, 20]: (a) shear deformation is negligible; (b) nonlinear warping and curvature effects are negligible in comparison to the midplane stretching nonlinearities; (c) ideally, the pedal will not be displaced along the X-axis due to symmetry; and, (d) the pedal is rigid relative to the beams.

The first two terms in the kinetic energy are for the beam flexural and torsional displacements. The rest of the terms in the kinetic energy are associated with translational (Y and Z directions) and rotational motions of the pedal mass M_p . The first two terms in the potential energy are for the flexural and torsional rigidities of the beams. Potential energy also includes gravitational effect and the nonlinear midplane stretching effect. The last two terms in potential energy are associated with electrostatic actuation electrode A and sensing electrode B. V_{ac} is the applied AC voltage with frequency Ω on electrode A. V_{b1} and V_{b2} are the bias voltages on electrodes A and B, respectively, and ϵ_0 is the permittivity of free space. The modes considered in this analysis do not result in a large rotation of the pedal about Z-axis and Y-axis. As a result, the rotations of the pedal about these axes are neglected in writing the electrostatic terms associated with electrode A voltages V_{b1} and V_{ac} .

The Lagrangian of the system in nondimensional form, denoted by $\hat{\mathcal{L}}$, can be written as follows:

$$\begin{aligned} \hat{\mathcal{L}} &= \frac{(T - U)L_1}{EI_1} \\ &= \sum_{i=1}^2 \left(\frac{1}{2} \nu_i \int_0^1 (\dot{\hat{v}}_i^2 + \dot{\hat{w}}_i^2) d\bar{s}_i + \frac{1}{2} \nu_i \kappa \int_0^1 \dot{\theta}_i^2 d\bar{s}_i \right) \\ &\quad + \frac{1}{2} R_p \left(\dot{\hat{v}}_1^2 + \dot{\hat{w}}_1^2 + \bar{b}_p \dot{\hat{v}}_1 \dot{\hat{v}}_1' + \frac{\bar{b}_p^2 + \nu_3^2}{3} \dot{\hat{v}}_1'^2 \right) \\ &\quad + \frac{\bar{b}_p^2}{3} \dot{\hat{w}}_1'^2 + \frac{\nu_3^2}{3} \dot{\theta}_1^2 + \nu_3 \dot{\hat{w}}_1 \dot{\theta}_1 + \bar{b}_p \dot{\hat{w}}_1 \dot{\hat{w}}_1' \\ &\quad + \frac{1}{2} \bar{b}_p \nu_3 \dot{\hat{w}}_1' \dot{\theta}_1 - \nu_3 \dot{\hat{v}}_1 \dot{\hat{v}}_1' \dot{\hat{v}}_1' \\ &\quad - \nu_3 \left(\dot{\hat{v}}_1 + \frac{\bar{b}_p}{2} \dot{\hat{v}}_1' \right) \dot{\theta}_1 \dot{\theta}_1 + \frac{1}{2} \nu_3 \bar{b}_p \dot{\hat{w}}_1' \dot{\hat{w}}_1' \dot{\hat{v}}_1' \\ &\quad + \frac{2}{3} \nu_3^2 (\dot{\hat{v}}_1 \dot{\hat{w}}_1' \dot{\theta}_1 + \dot{\hat{v}}_1' \dot{\hat{w}}_1 \dot{\theta}_1) \Big|_{\bar{s}_1=1} \end{aligned}$$

$$\begin{aligned} &- \sum_{i=1}^2 \left(\frac{1}{2\nu_i^3} \int_0^1 (\hat{v}_i'^2 + \bar{I} \hat{w}_i'^2) d\bar{s}_i \right. \\ &\quad \left. + \frac{\gamma}{2\nu_i} \int_0^1 \theta_i'^2 d\bar{s}_i \right) - R_p \bar{g} \left(\hat{w}_1 + \frac{\bar{b}_p}{2} \hat{w}_1' \right. \\ &\quad \left. + \frac{\nu_3}{2} \theta_1 \right) \Big|_{\bar{s}_1=1} - \frac{1}{8} \frac{S}{\nu_1 + \nu_2} \left(\left(\sum_{i=1}^2 \int_0^1 \frac{\hat{v}_i'^2}{\nu_i} d\bar{s}_i \right)^2 \right. \\ &\quad \left. + \left(\sum_{i=1}^2 \int_0^1 \frac{\hat{w}_i'^2}{\nu_i} d\bar{s}_i \right)^2 \right) + (F_0 + F_1 \cos \bar{\Omega} \tau) \\ &\quad + F_2 \cos 2\bar{\Omega} \tau \left(\frac{\bar{b}_p}{1 + (\hat{v}_1|_{\bar{s}_1=1})/g_1} \right. \\ &\quad \left. + \sum_{i=1}^2 \nu_i \int_{1-\bar{l}_i}^1 \frac{1}{1 + \hat{v}_i/g_1} d\bar{s}_i \right) \\ &\quad + G_0 \nu_3 \int_{1-\bar{l}_3}^1 \frac{1}{1 + \frac{1}{g_2} (\hat{w}_1 + \bar{s}_3 \nu_3 \theta_1)|_{\bar{s}_1=1}} d\bar{s}_3, \end{aligned} \tag{2}$$

where the following nondimensional parameters are introduced:

$$\begin{aligned} \hat{v}_i &= \frac{v_i}{L_1}, & \hat{w}_i &= \frac{w_i}{L_1}, & \nu_i &= \frac{L_i}{L_1}, & \nu_3 &= \frac{L_p}{L_1}, \\ \bar{s}_i &= \frac{s_i}{L_i}, & \bar{s}_3 &= \frac{s_3}{L_p}, \\ \kappa &= \frac{b^2 + h^2}{12L_1^2}, & R_p &= \frac{M_p}{m_b L_1}, \\ \gamma &= \frac{GK}{EI}, & S &= \frac{bhL_1^2}{I_1}, \\ \bar{l}_i &= \frac{l_i}{L_i}, & \bar{l}_3 &= \frac{l_3}{L_p}, \\ g_i &= \frac{d_i}{L_1}, & \bar{b}_p &= \frac{b_p}{L_1}, \\ \tau &= \sqrt{\frac{EI}{m_b L_1^4}} t, & \bar{\Omega} &= \Omega \sqrt{\frac{m_b L_1^4}{EI}}, \\ \bar{g} &= g \frac{m_b L_1^3}{EI_1}, & \bar{I} &= \frac{I_2}{I_1}, \\ [F_0, F_1, F_2]^t &= \frac{L_1}{EI} \frac{\epsilon_0 b L_1}{2d_1} \\ &\quad \times [V_{b1}^2 + 0.5V_{ac}^2, 2V_{b1} V_{ac}, 0.5V_{ac}^2]^t, \end{aligned} \tag{3}$$

$$G_0 = \frac{L_1}{EI} \frac{\epsilon_0 b_p L_1}{2d_2} v_2^2.$$

In (2), a dot now denotes derivative with respect to nondimensional time τ , and a prime denotes derivative with respect to the appropriate nondimensional arc length \bar{s}_i . Since the beam lengths are normalized with respect to length L_1 of beam 1, the length ratio v_1 is unity. The length ratio v_2 for beam 2 is unity when the beams 1 and 2 have the same length.

3 Linear equations of motion

We now perform a linear analysis to compute the mode shapes and natural frequencies of the structure. This will define conditions on parameters needed to assure 1:2 resonance between the torsional and flexural modes of the structure.

The Lagrangian in (2) with only quadratic terms can be used along with Hamilton's principle to derive the nondimensional linear equations of motion. The resulting linear equations of motion without the gravity force due to pedal mass and electrostatic capacitive effects are as follows:

$$\begin{aligned} v_i \ddot{v}_i + \frac{1}{v_i^3} \hat{v}_i'''' &= 0, \\ v_i \ddot{w}_i + \frac{\bar{I}}{v_i^3} \hat{w}_i'''' &= 0, \\ v_i \kappa \ddot{\theta}_i - \frac{\gamma}{v_i} \theta_i'' &= 0, \quad i = 1, 2. \end{aligned} \quad (4)$$

The associated geometric and natural boundary conditions for the linear problem are described next. The assumption that the beams 1 and 2 are clamped at, respectively, $\bar{s}_1 = 0$ and $\bar{s}_2 = 0$, results in the following geometric boundary conditions:

$$\left. \begin{aligned} \hat{v}_i|_{\bar{s}_i=0} &= 0, & \hat{v}_i'|_{\bar{s}_i=0} &= 0, & \hat{w}_i|_{\bar{s}_i=0} &= 0, \\ \hat{w}_i'|_{\bar{s}_i=0} &= 0, & \theta_i|_{\bar{s}_i=0} &= 0, & i &= 1, 2. \end{aligned} \right\} \quad (5)$$

Since the pedal structure is assumed to be rigid for the modes considered in this analysis, the beams slopes

and displacements at $\bar{s}_1 = 1$ and $\bar{s}_2 = 1$ are constrained as follows:

$$\begin{aligned} \theta_1|_{\bar{s}_1=1} &= \theta_2|_{\bar{s}_2=1}, \\ (\hat{v}_1 + \bar{b}_p \hat{v}_1')|_{\bar{s}_1=1} &= \hat{v}_2|_{\bar{s}_2=1}, \\ v_2 \hat{v}_1'|_{\bar{s}_1=1} &= -\hat{v}_2'|_{\bar{s}_2=1}, \\ (\hat{w}_1 + \bar{b}_p \hat{w}_1')|_{\bar{s}_1=1} &= \hat{w}_2|_{\bar{s}_2=1}, \\ v_2 \hat{w}_1'|_{\bar{s}_1=1} &= -\hat{w}_2'|_{\bar{s}_2=1}. \end{aligned} \quad (6)$$

The natural boundary conditions can be derived either by force and moment balances at the pedal or by introducing the geometric constraints at the pedal end, (6), in the Lagrangian using Lagrange multipliers and applying the Hamilton's principle. The resulting natural boundary conditions are:

$$\begin{aligned} \left(R_p \ddot{v}_1 + \frac{1}{2} R_p \bar{b}_p \ddot{v}_1' - \hat{v}_1'''' \right) \Big|_{\bar{s}_1=1} &= \frac{\hat{v}_2''''}{v_2^3} \Big|_{\bar{s}_2=1}, \\ \left(\frac{1}{3} R_p (\bar{b}_p^2 + v_3^2) \ddot{v}_1' + \frac{1}{2} R_p \bar{b}_p \ddot{v}_1 + \hat{v}_1'' \right) \Big|_{\bar{s}_1=1} \\ &= \left(\frac{\hat{v}_2''}{v_2^2} + \bar{b}_p \frac{\hat{v}_2''''}{v_2^3} \right) \Big|_{\bar{s}_2=1}, \\ \left(R_p \left(\frac{v_3^2}{3} \ddot{\theta}_1 + \frac{v_3}{2} \ddot{w}_1 + \frac{\bar{b}_p v_3}{4} \ddot{w}_1' \right) + \gamma \theta_1' \right) \Big|_{\bar{s}_1=1} \\ &= -\frac{\gamma}{v_2} \theta_2' \Big|_{\bar{s}_2=1}, \\ \left(R_p \left(\ddot{w}_1 + \frac{v_3}{2} \ddot{\theta}_1 + \frac{\bar{b}_p}{2} \ddot{w}_1' \right) - \bar{I} \hat{w}_1'''' \right) \Big|_{\bar{s}_1=1} \\ &= \frac{\bar{I}}{v_2^3} \hat{w}_2'''' \Big|_{\bar{s}_2=1}, \\ \left(R_p \left(\frac{\bar{b}_p}{2} \ddot{w}_1 + \frac{\bar{b}_p^2}{3} \ddot{w}_1' + \frac{\bar{b}_p v_3}{4} \ddot{\theta}_1 \right) + \bar{I} \hat{w}_1'' \right) \Big|_{\bar{s}_1=1} \\ &= \frac{\bar{I}}{v_2^2} \left(\hat{w}_2'' + \frac{\bar{b}_p}{v_2} \hat{w}_2'' \right) \Big|_{\bar{s}_2=1}. \end{aligned} \quad (7)$$

Note that in the linear equations of motion (4) and the boundary conditions (5)–(7), the in-plane bending motion is uncoupled from the torsional and out-of-plane bending motions of the structure. However, the out-of-plane bending and torsional motion are coupled through the pedal inertia.

The linear mode shapes and natural frequencies of the structure are obtained by assuming the solution in

following form:

$$\begin{aligned} \hat{v}_i(\bar{s}_i, \tau) &= (\lambda_{1i}(\cos \beta_{fi}\bar{s}_i - \cosh \beta_{fi}\bar{s}_i) \\ &\quad + \lambda_{2i}(\sin \beta_{fi}\bar{s}_i - \sinh \beta_{fi}\bar{s}_i))e^{(J\omega\tau)}, \\ \hat{w}_i(\bar{s}_i, \tau) &= (\lambda_{3i}(\cos \beta_{oi}\bar{s}_i - \cosh \beta_{oi}\bar{s}_i) \\ &\quad + \lambda_{4i}(\sin \beta_{oi}\bar{s}_i - \sinh \beta_{oi}\bar{s}_i))e^{(J\omega\tau)}, \end{aligned} \tag{8}$$

$$\theta_i(\bar{s}_i, \tau) = (\lambda_{5i} \sin \beta_{ti}\bar{s}_i)e^{(J\omega\tau)}, \quad i = 1, 2,$$

where $J = \sqrt{-1}$, and β_{fi} , β_{oi} , and β_{ti} are defined as:

$$\begin{aligned} \beta_{fi} &= v_i \sqrt{\omega}, & \beta_{oi} &= \frac{v_i}{(\bar{I})^{1/4}} \sqrt{\omega}, \\ \beta_{ti} &= \sqrt{\frac{\kappa}{\gamma}} v_i \omega, & i &= 1, 2. \end{aligned} \tag{9}$$

Note that the assumed solution satisfies the geometric boundary conditions at $\bar{s}_i = 0$ in (5). The ten unknown coefficients, $\lambda_{1-5 i}$ with $i = 1, 2$, defining the mode shapes are then determined by the characteristic matrix generated by the remaining ten boundary conditions in (6) and (7).

The natural frequencies and mode shapes of the pedal structure depend on geometric as well as material parameters of the model. As an example, consider a pedal resonator with dimensions:

$$\begin{aligned} L_1 &= 100 \mu\text{m}, & L_2 &= 100 \mu\text{m}, \\ h &= 3 \mu\text{m}, & b &= 5 \mu\text{m}, \\ b_p &= 25 \mu\text{m}, & d_1 &= 2 \mu\text{m}, & d_2 &= 2 \mu\text{m}. \end{aligned} \tag{10}$$

The resonator is assumed to be made of polysilicon. The properties of polysilicon material [21] are assumed to be: Young’s modulus $E = 170$ GPa, density $\rho = 2330$ kg/m³, and Poisson’s ratio $\nu = 0.22$. The lowest natural frequencies of the pedal resonator can be then computed and are plotted in Fig. 2 as a function of the pedal length L_p . This allows us to identify the pedal length L_p for which the lowest torsional mode natural frequency is half of the lowest in-plane flexural mode frequency. From Fig. 2, the two frequencies are closest to 1:2 ratio when $L_p = 102 \mu\text{m}$. The first two natural frequencies for the design pedal length, $L_p = 102 \mu\text{m}$, are 95.041 kHz (in torsion) and 189.695 kHz (in flexure), and the mistuning from 1:2 internal resonance between the modes is $\sim 0.2\%$. We will later see that this mismatch can be eliminated by proper application of electrostatic bias voltages on electrodes A and B.

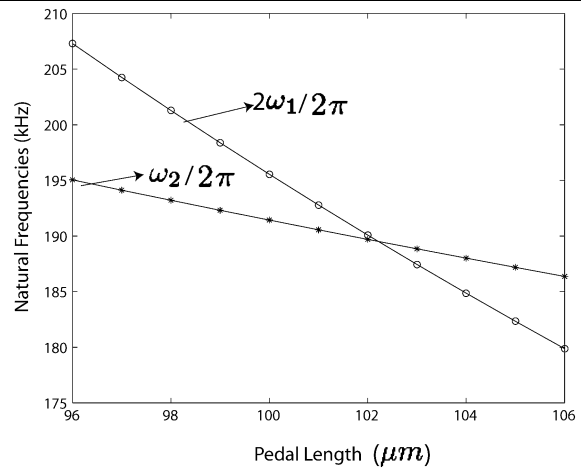


Fig. 2 Variation of the natural frequency of the in-plane flexural mode (ω_2), and two times the natural frequency of the torsional mode (ω_1), as a function of the pedal length L_p

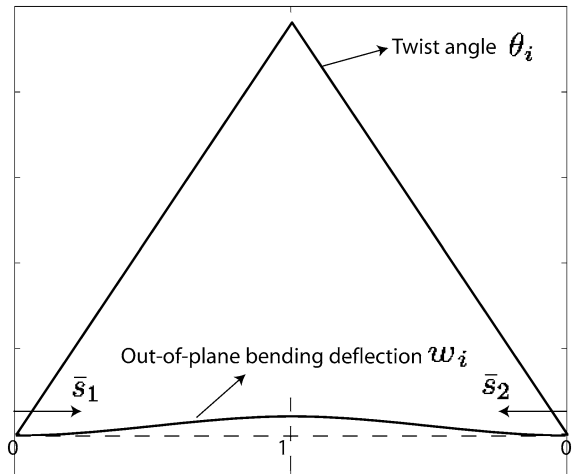


Fig. 3 The angular twists of beams 1 and 2, and the accompanying out-of-plane flexural deflections, in the lowest torsional mode of the microresonator with natural frequency 93.478 kHz

The first mode shape for the resonator with dimensions in (10) and pedal length $L_p = 102 \mu\text{m}$ is shown in Fig. 3. It shows the angular deflections and out-of-plane bending deflections of the beams 1 and 2. In this mode shape, the pedal primarily moves because of the torsional angular deflections. There is a very small, though nonzero, component of out-of-plane flexural motion. As a result, we refer this mode as torsional mode shape. In the torsional mode computed by linear analysis, the beams do not deflect in Y-direction since in-plane bending motions are uncoupled from the torsional and out-of-plane bending motions. Note that the

torsional angular deflections are almost a linear function of the beam arc lengths \bar{s}_i , which is a result of the pedal mass being much larger than the total beam mass and the beams being relatively slender. Figure 4 shows the beam deflections in Y direction corresponding to the resonator’s second mode where the beams are only in flexure. In this flexural mode, the coefficients for beam out-of-plane bending deflections and twist angles, $\lambda_{3-51}, \lambda_{3-52}$ in (8), are identically zero. Thus, the beams only deflect in Y direction with no twisting, as is expected.

Figures 5(a) and (b) show the torsional and flexural modes of the same pedal resonator, as predicted by a finite element model (3-D brick model) developed in ANSYS. For this model, 3-D 20 node structural solid elements (solid95) were used. The torsional mode natural frequency for the FEM model is 91.4 kHz. FEM generated torsional mode shape in Fig. 5(a) is in excellent agreement with the analytically computed mode

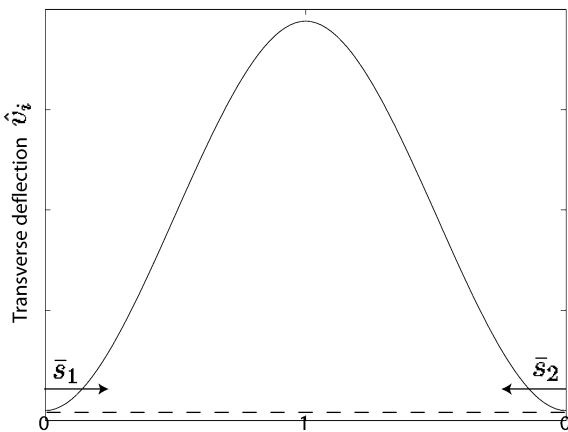
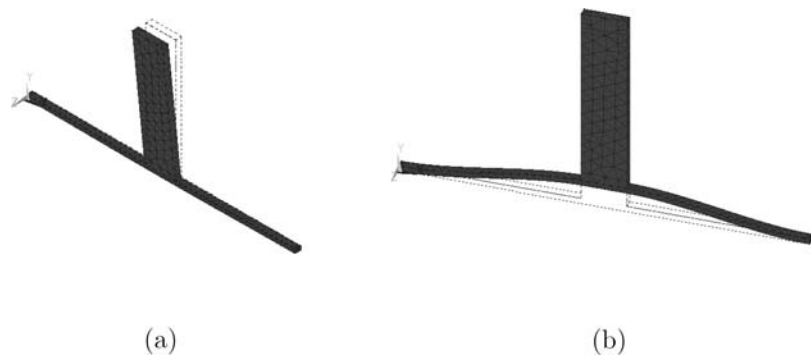


Fig. 4 The flexural deflections of the two beams for in-plane flexural mode of the microresonator with natural frequency 186.365 kHz. The beams only undergo transverse deflections with no twist

Fig. 5 The first two linear modes of the pedal microresonator, as predicted by the finite element package ANSYS. (a) The first mode is with the two beams in torsion about the X-axis; (b) the second mode is with both beams in flexure in XY plane



shape, with the beams showing no deflection in Y direction and only a very small deflection in Z direction. For the flexural mode, the prediction by the ANSYS model is shown in Fig. 5(b) and the computed natural frequency is 182.4 kHz. In the flexural mode, as is confirmed by the FEM model, the beams do not undergo any torsional deflection and as a result, the pedal structure moves only in Y direction.

The lowest mode in which out-of-plane bending deflection, along with torsional motion, contribute significantly is also obtained analytically as well as using ANSYS. The resulting ANSYS mode shape which matches with analytical mode shape is shown in Fig. 6. The analytical natural frequency of this mode for the example resonator is 586.1 kHz. In this mode shape, the bending and torsional deflection of the beam are in out-of-phase. The spatial configuration of applied electrostatic force through pedal electrode limits the contribution of this out-of-phase mode shape in the pedal response.

4 Two-mode reduced-order model

In steady state nonlinear response of the system, modes not excited directly or indirectly through internal resonance are expected to decay due to the presence of damping [7]. As a result, the resonator angular and flexural deflections are assumed to be of the form:

$$\begin{aligned} \theta_i(\bar{s}_i, \tau) &= \Phi_{ti}(\bar{s}_i)A_1(\tau), \\ \hat{w}_i(\bar{s}_i, \tau) &= \Phi_{oi}(\bar{s}_i)A_1(\tau), \\ \hat{v}_i(\bar{s}_i, \tau) &= \Phi_{fi}(\bar{s}_i)A_2(\tau), \quad i = 1, 2, \end{aligned} \tag{11}$$

where Φ_{ti} and Φ_{oi} are torsional and out-of-plane bending deflection of i 'th beam, respectively, in torsional mode. Φ_{fi} is the deflection of i 'th beam in

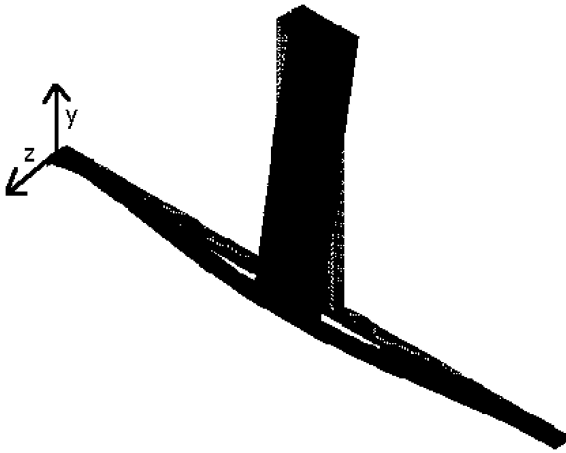


Fig. 6 The lowest out-of-plane bending mode, with out-of-phase torsional angular deflection and out-of-plane bending deflection, as predicted by the finite element package ANSYS

in-plane bending mode. A_1 and A_2 are functions of time that represent the torsional and in-plane bending modal amplitudes, respectively. Analytically computed mode shapes, as described in linear analysis, are used in the above expansion.

We also include the effect of placing a mass particle on the resonator; say, a particle of mass M_t placed in the middle of the tip of the pedal. Such a situation can occur when the resonator is used for sensing, or the mass particle is used to change the natural frequencies and thereby tuning the structural system to bring the resonator to exact 1:2 internal resonance. The particle mass is assumed to be small so that the mode shapes are not changed. The particle will result in changing the kinetic energy and gravitational potential energy of the structure. The additional kinetic and potential energy of the particle, \hat{T}_{M_t} and \hat{U}_{M_t} , respectively, nondimensionalized by EI/L_1 , are given as follows:

$$\begin{aligned} \hat{T}_{M_t} = & \frac{1}{2} R_t R_p \left(\dot{v}_1^2 + \dot{w}_1^2 + \bar{b}_p \dot{v}_1 \dot{v}'_1 + (\bar{b}_p^2/4 + v_3^2) \dot{v}_1^{\prime 2} \right. \\ & + \frac{\bar{b}_p^2}{4} \dot{w}_1^{\prime 2} + v_3^2 \dot{\theta}_1^2 + 2v_3 \dot{w}_1 \dot{\theta}_1 + \bar{b}_p \dot{w}_1 \dot{w}'_1 \\ & + \bar{b}_p v_3 \dot{w}_1 \dot{\theta}_1 - 2v_3 \dot{v}_1 \dot{v}'_1 \\ & - 2v_3 \left(\dot{v}_1 + \frac{\bar{b}_p}{2} \dot{v}'_1 \right) \theta_1 \dot{\theta}_1 + v_3 \bar{b}_p \dot{w}_1 \dot{w}'_1 \dot{v}'_1 \\ & \left. + 2v_3^2 (\dot{v}'_1 \dot{w}'_1 \theta_1 + \dot{v}_1 \dot{w}'_1 \dot{\theta}_1) \right) \Big|_{\bar{s}_1=1}, \end{aligned} \tag{12}$$

$$\hat{U}_{M_t} = R_p R_t \bar{g} \left(\hat{w}_1 + \frac{\bar{b}_p}{2} \hat{w}'_1 + v_3 \theta_1 \right) \Big|_{\bar{s}_1=1},$$

where $R_t = M_t/M_p$ is the nondimensionalized mass of the particle.

Substituting the expressions in (11) in the Lagrangian with tip mass, (2) and (12), the following Lagrange's equations governing the modal amplitudes are obtained:

$$\begin{aligned} \ddot{A}_1 + 2\zeta_1 \omega_1 \dot{A}_1 + \omega_1^2 A_1 \\ = -\bar{g} R_0 - k_{31} A_1^3 + \frac{\alpha}{R_1} A_1 \ddot{A}_2 + \frac{G_0}{R_1} \sum_{k=0}^n h_k \frac{A_1^k}{g_2^{k+1}}, \\ \ddot{A}_2 + 2\zeta_2 \omega_2 \dot{A}_2 + \omega_2^2 A_2 \\ = -k_{32} A_2^3 + \frac{\alpha}{R_2} (\dot{A}_1^2 + \ddot{A}_1 A_1) + \frac{\Gamma}{R_2} (\dot{A}_2^2 + 2A_2 \ddot{A}_2) \end{aligned} \tag{13}$$

$$\begin{aligned} & + \frac{1}{R_2} (F_0 + F_1 \cos \bar{\Omega} \tau \\ & + F_2 \cos 2\bar{\Omega} \tau) \sum_{k=0}^n f_k \frac{A_2^k}{g_1^{k+1}}, \end{aligned}$$

$$\omega_1^2 = \frac{1}{R_1} \sum_{i=1}^2 \int_0^1 \left(\frac{\gamma}{v_i} \Phi_{ii}^{\prime 2} + \frac{\bar{I}}{v_i^3} \Phi_{oi}^{\prime 2} \right) d\bar{s}_i,$$

$$\omega_2^2 = \frac{1}{R_2} \sum_{i=1}^2 \int_0^1 \frac{1}{v_i^3} \Phi_{fi}^{\prime 2} d\bar{s}_i,$$

$$\begin{aligned} R_1 = & R_p \left(\frac{v_3^2}{3} (1 + 3R_t) \Phi_{t1}^2 \right. \\ & + (1 + R_t) (\Phi_{o1}^2 + \bar{b}_p \Phi_{o1} \Phi'_{o1}) \\ & + \left(\frac{\bar{b}_p^2}{3} + R_t \frac{\bar{b}_p^2}{4} \right) \Phi_{o1}^{\prime 2} \\ & + (1 + 2R_t) \\ & \left. \times \left(v_3 \Phi_{o1} \Phi_{t1} + \frac{1}{2} \bar{b}_p v_3 \Phi_{t1} \Phi'_{o1} \right) \right) \Big|_{\bar{s}_1=1} \end{aligned}$$

$$+ \kappa \sum_{i=1}^2 \int_0^1 v_i (\Phi_{ii}^2 + \Phi_{oi}^2) d\bar{s}_i,$$

$$\begin{aligned} R_2 = & R_p (1 + R_t) (\Phi_{f1}^2 + \bar{b}_p \Phi_{f1} \Phi'_{f1}) \Big|_{\bar{s}_1=1} \\ & + \frac{1}{3} R_p (\bar{b}_p^2 + v_3^2) \Phi_{f1}^{\prime 2} \Big|_{\bar{s}_1=1} \\ & + R_p R_t (\bar{b}_p^2/4 + v_3^2) \Phi_{f1}^{\prime 2} \Big|_{\bar{s}_1=1} \end{aligned}$$

$$\begin{aligned}
& + \sum_{i=1}^2 \int_0^1 v_i \Phi_{f_i}^2 d\bar{s}_i, \\
R_0 &= \frac{R_p}{R_1} \left(\frac{v_3}{2} (1 + 2R_t) \Phi_{t1} \right. \\
& \quad \left. + (1 + R_t) \left(\Phi_{o1} + \frac{\bar{b}_p}{2} \Phi'_{o1} \right) \right) \Big|_{\bar{s}_1=1}, \\
\alpha &= \frac{1}{2} R_p v_3 \left((1 + 2R_t) \left(\Phi_{f1} \Phi_{t1}^2 + \frac{\bar{b}_p}{2} \Phi'_{f1} \Phi_{t1}^2 \right. \right. \\
& \quad \left. \left. - \frac{1}{2} \bar{b}_p v_3 \Phi'_{f1} \Phi_{o1}^2 \right) \right. \\
& \quad \left. - \frac{4}{3} (1 + 6R_t) v_3 \Phi'_{f1} \Phi'_{o1} \Phi_{t1} \right) \Big|_{\bar{s}_1=1}, \\
\Gamma &= \frac{1}{2} R_p (1 + 2R_t) v_3 \left(\Phi_{f1} \Phi_{f1}^2 \right) \Big|_{\bar{s}_1=1}, \\
k_{31/2} &= \frac{1}{2} \frac{S}{v_1 + v_2} \left(\sum_{i=1}^2 \int_0^1 \frac{\Phi_{o/fi}^2}{v_i} d\bar{s}_i \right)^2, \\
f_k &= (-1)^{k+1} (k+1) \left(\bar{b}_p \Phi_{f1}^{k+1} (1) \right. \\
& \quad \left. + \sum_{i=1}^2 v_i \int_{1-\bar{l}_i}^1 \Phi_{fi}^{k+1} d\bar{s}_i \right), \\
h_k &= (-1)^{k+1} \frac{k+1}{(k+2) \Phi_{t1}} \left((\Phi_{o1} + v_3 \Phi_{t1})^{k+2} \right. \\
& \quad \left. - (\Phi_{o1} + v_3 (1 - \bar{l}_3) \Phi_{t1})^{k+2} \right) \Big|_{\bar{s}_1=1}, \\
k &= 0, 1, \dots, n, \tag{14}
\end{aligned}$$

and ζ_1 and ζ_2 are the modal dampings introduced for torsional mode and flexural mode, respectively. Also, ω_1 and ω_2 are, respectively, the nondimensional natural frequencies of the torsional and the flexural modes, and α is the coefficient of inertial quadratic nonlinearities coupling the flexural and the torsional modal amplitudes. Γ is the coefficient of inertial quadratic nonlinearities affecting the flexural modal amplitude, which arise due to the in-plane rotation of the pedal about Z axis. k_{31} and k_{32} are the coefficients of cubic nonlinearities due to stretching of neutral axis. R_1 and R_2 are the modal masses for the torsional and the flexural modes, respectively. Note that the modal mass R_2 includes the inertia contribution of the in-plane rotation of the pedal due to a nonzero slope of the transverse beam displacement at the pedal end. $\bar{g}R_0$ is the nondimensional gravity

force. Parameters f_k and h_k in the electrostatic actuation terms are introduced to keep the equations of motion concise. Note that the electrostatic potential terms are approximated to n th order by Taylor series expansion, which resulted in electrostatic actuation parameters f_k and h_k .

In the actuation terms corresponding to electrostatic forces, nonlinearities up to order n are retained. Higher-order actuation nonlinearities will be utilized primarily for calculating static pull-in voltages [5, 22, 23]. Further note that in equation of motion for the flexural modal amplitude A_2 , the nonlinearity in electrostatic actuation results in parametric excitation effect as well in addition to the direct excitation of the flexural mode.

5 Static equilibrium solution

As is expected, static forces due to bias voltages and the pedal weight result in deflecting the beams and the pedal structure from zero equilibrium position. The equations governing static equilibrium of the structural system can be obtained from equations of motion, (13), by setting the time derivatives and the AC voltage contributions F_1 and F_2 to zero. The resulting equations are:

$$\begin{aligned}
\omega_1^2 A_{10} &= -\bar{g}R_0 - k_{31} A_{10}^3 + \frac{G_0}{R_1} \sum_{k=0}^n h_k \frac{A_{10}^k}{g_2^{k+1}}, \\
\omega_2^2 A_{20} &= -k_{32} A_{20}^3 + \frac{F_0}{R_2} \sum_{k=0}^n f_k \frac{A_{20}^k}{g_1^{k+1}}, \tag{15}
\end{aligned}$$

where A_{10} and A_{20} are the modal amplitudes in static equilibrium. Equations (15) are uncoupled nonlinear equations for the deflection amplitudes A_{10} and A_{20} . This shows that the bias voltage, embedded in parameter G_0 , on electrode B beneath the pedal does not cause any deflection in Y-direction. Similarly, the bias voltage on the lateral electrode A, embedded in parameter F_0 , results in an in-plane deflection of the beams (in Y-direction) with no out-of-plane displacements of the pedal. Since (15) are nonlinear, they can possess multiple equilibrium solutions as a function of bias voltages. We can also use these equations to predict static pull-in voltages for the pedal resonator. Here, by a ‘‘pull-in’’ voltage, we refer to the voltage beyond which there is a jump in the gradually increasing static deflection position to where the deflection increases

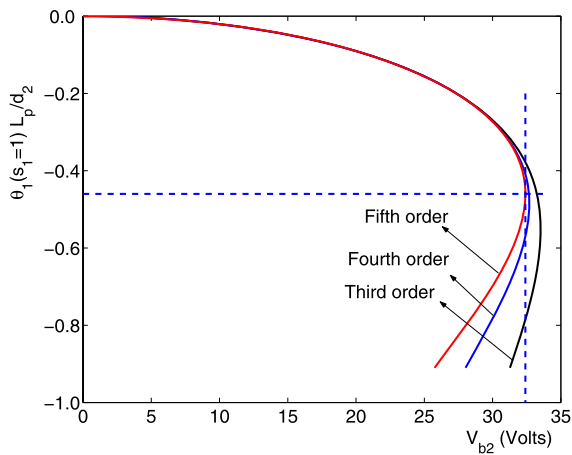


Fig. 7 The ratio of out-of-plane static deflection of the resonator at the tip of the pedal ($\theta_1(s_1 = 1)L_p$) to the electrode B gap d_2 , as a function of the electrode B bias voltage V_{b2} . The vertical dashed line indicates the pull-in voltage for the model retaining fifth order nonlinear electrostatic terms, and the horizontal dashed line indicates the corresponding pull-in deflection

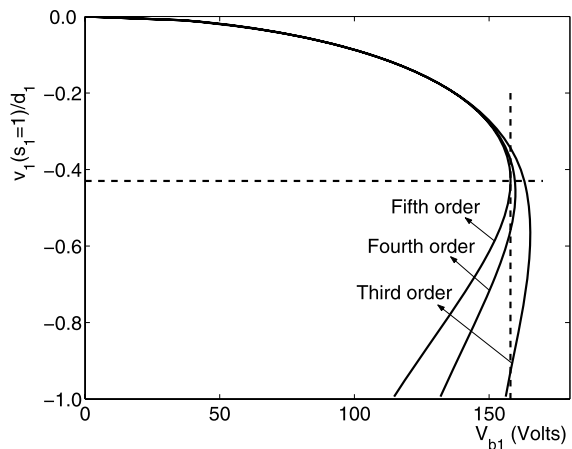


Fig. 8 The ratio of transverse static deflection of the resonator at the end of the beam 1 ($v_1(s_1 = 1)$) to the lateral electrode gap d_1 , as a function of the electrode B bias voltage V_{b1} . The vertical dashed line indicates the pull-in voltage for the model retaining fifth order nonlinear electrostatic terms, and the horizontal dashed line indicates the corresponding pull-in deflection

unboundedly. Note that there are two possible pull-in voltages independent of each other, one for the flexural in-plane deflection and the other for torsional out-of-plane deflection.

Figures 7 and 8 show, respectively, the nondimensional deflections ($\theta_1|_{s_1=1} L_p/d_2$) and ($v_1|_{s_1=1} L_1/d_1$) as functions of the bias voltages V_{b2} (on electrode B)

and V_{b1} (on electrode A). Note that ($\theta_1|_{s_1=1} L_p$) is the out-of-plane (Z-direction) pedal tip displacement with beams in torsion, and ($v_1|_{s_1=1} L_1$) is the transverse (in-plane) beam 1 displacement at the pedal end, $s_1 = 1$. For results in these and later figures, the electrodes are assumed to span the whole length of the beams and the pedal, that is, $\bar{l}_1 = \bar{l}_2 = \bar{l}_3 = 1$. These are computed by using the mode shapes obtained in the linear analysis above and (15). The structure is assumed to have no tip mass. To see the effect of including nonlinear actuation terms of different order, the deflection vs. voltage curves are shown for models that retain nonlinear actuation terms up to third, fourth, and fifth orders. Clearly, in both the figures, as the bias voltage increases, the nonlinear terms become more important.

Note that for some bias voltage values, as expected, there are more than one possible equilibrium deflections. Physically, when the bias voltages are small and are slowly increased starting from zero, the deflections are on the solution branch close to the zero equilibrium. The pull-in voltages can be obtained from the plots by identifying the voltage for which the two solution branches merge or the slope of the solution curve is ∞ . The resulting pull-in voltages, $(V_{b1})_{pi}$ and $(V_{b2})_{pi}$, for this resonator using the model that retains fifth-order actuation nonlinearities are:

$$(V_{b1})_{pi} = 158 \text{ Volts}, \quad (V_{b2})_{pi} = 32.4 \text{ Volts}. \quad (16)$$

For the case of clamped-clamped beam, the pull-in voltage [23] is 168 Volts with the electrodes spanning the beam lengths. The torsional pull-in voltage ($V_{b2})_{pi}$ using the formula by Degani et al. [22], which accounts only for the torsional energy of the pedal, is 32 Volts. Thus, the pull-in voltage values presented here are in good agreement with published results.

For the example resonator, the deflection of pedal tip due to gravity (41 pico m) is much smaller than the deflection due to electrostatic forces. The contribution of out-of-plane bending in pedal tip deflection, determined by the mode shape of the resonator, is 4.4%. In a related study of a symmetric torsional mirror, Daqaq [24, 25] concluded that as the ratio of bending stiffness to the torsional stiffness increases, the pull-in voltage increases. The study also detailed the effect of electrode length on pull-in voltage. They also studied the response of the structure when the torsional mode and out-of-plane bending mode are in 1:2 internal resonance, and the lower frequency torsional mode is excited in resonance. However, a symmetric torsional

mirror structure does not have the same quadratic nonlinearities as the pedal structure discussed in this paper. Further, unlike the out-of-plane bending and torsional mode interaction in [24], the interacting modes in this study are in-plane bending mode and the torsional mode.

In the nonlinear resonator mode of operation considered in this work, we focus on small bias voltages which are much lower than the pull-in voltages. The corresponding equilibrium positions or deflections are represented by the upper branch of the roots of these equations and can be obtained by assuming a power series solution for A_{10} and A_{20} in terms of gravity and electrostatic actuation terms (F_0 and G_0). The resulting equilibrium solutions are given by:

$$A_{10} = -\bar{g} \frac{R_0}{\omega_1^2} + \frac{h_0}{\omega_1^2 g_2} \frac{G_0}{R_1} + O(G_0^2),$$

$$A_{20} = \frac{f_0}{\omega_2^2 g_1} \frac{F_0}{R_2} + O(F_0^2).$$
(17)

The equilibrium solutions in (17) clearly show the dependence of out-of-plane and in-plane deflections of the pedal structure on the bias voltages applied to electrode B and to electrode A.

6 Dynamic response formulation and asymptotic equations

The oscillatory response of the structure about an equilibrium position is of utmost interest in the resonator applications. The total resonator response comprises of the static deflection and the time-dependent motion about the static equilibrium. As a result, we assume the following form of the modal amplitudes A_1 and A_2 :

$$A_i(\tau) = A_{i0} + a_i(\tau), \quad i = 1, 2, \tag{18}$$

where a_1 and a_2 denote the time-dependent components of the modal amplitudes A_1 and A_2 , respectively.

In order to study the response analytically, we apply the method of averaging [7] to obtain slow evolution equations that govern the approximate asymptotic response of the nonlinear microresonator when subjected to harmonic electrostatic actuation of the flexural in-plane mode of oscillation. The equations of motion (13) need to be first appropriately scaled and transformed to the standard-form [7, 26] in the method

of averaging. We scale the angular and transverse displacement modal amplitudes, a_1 and a_2 , respectively, and modal dampings and actuation forces, using a dimensionless parameter ϵ , with $0 < \epsilon \ll 1$, as follows:

$$a_i = \epsilon \hat{a}_i, \quad \zeta_i = \epsilon \hat{\zeta}_i, \quad F_i = \epsilon^2 \hat{F}_i,$$

$$G_0 = \epsilon \hat{G}_0, \quad F_0 = \epsilon \hat{F}_0, \quad i = 1, 2. \tag{19}$$

These scalings in (19) along with the static equilibrium solutions, (17), when substituted in equations of motion (13) order the various linear and nonlinear terms in the scaling parameter ϵ . To obtain a first-order asymptotic approximation to the resonator response, terms up to order ϵ^2 are retained in the equations of motion. The resulting equations of motion in terms of the scaled parameters are as follows:

$$\ddot{\hat{a}}_1 + \omega_1^2 \hat{a}_1 = \epsilon \left(\frac{\hat{G}_0}{R_1} \frac{h_1}{g_2^2} \hat{a}_1 - 2\hat{\zeta}_1 \omega_1 \dot{\hat{a}}_1 - \frac{\alpha}{R_1} \omega_2^2 \hat{a}_1 \hat{a}_2 \right. \\ \left. - \frac{\alpha}{R_1} \frac{\hat{G}_0}{R_1} \frac{h_0 \omega_2^2}{\omega_1^2 g_2} \hat{a}_2 \right) + O(\epsilon^2),$$

$$\ddot{\hat{a}}_2 + \omega_2^2 \hat{a}_2 = \epsilon \left(\frac{\hat{F}_0}{R_2} \frac{f_1}{g_1^2} \hat{a}_2 - 2\hat{\zeta}_2 \omega_2 \dot{\hat{a}}_2 \right. \\ \left. + \frac{\alpha}{R_2} \left(\dot{\hat{a}}_1^2 - \omega_1^2 \hat{a}_1^2 - \frac{\hat{G}_0}{R_1} \frac{h_0}{g_2} \hat{a}_1 \right) \right. \\ \left. + \frac{\Gamma}{R_2} \left(-2 \frac{\hat{F}_0 f_0}{g_1 R_2} \hat{a}_2 - 2\omega_2^2 \hat{a}_2^2 + \dot{\hat{a}}_2^2 \right) \right. \\ \left. + \frac{1}{R_2} \left(\hat{F}_1 \cos \bar{\Omega} \tau + \hat{F}_2 \cos 2\bar{\Omega} \tau \right) \frac{f_0}{g_1} \right) \\ + O(\epsilon^2). \tag{20}$$

6.1 Sensitivity of the natural frequencies

As shown earlier, the microresonator natural frequencies ω_1 and ω_2 of the lowest torsional and flexural modes can be chosen by adjusting the structural dimensions such that they are in 1:2 ratio. The resonator’s natural frequencies can be different from the designed (or nominal) microresonator due to many reasons, e.g., the addition of a mass particle if the resonator is used as a mass sensor, or due to fabrication uncertainties. First, consider the changes in pedal length and beam lengths from the nominal dimensions, as follows:

$$v_2 = (v_2)_c + \epsilon \Delta v_2, \quad v_3 = (v_3)_c + \epsilon \Delta v_3, \tag{21}$$

where $()_c$ will now denote the critical dimensions determined by linear analysis for which linear torsional and flexural modes of the microresonator are in exact 1:2 internal resonance. Δv_2 and Δv_3 in the above equations account for changes in the ratio of the beam lengths and the pedal length, respectively. We further scale the nondimensionalized particle mass R_t as $R_t = \epsilon \hat{R}_t$ to explicitly state that the particle mass is much smaller compared to the pedal mass and the nominal/critical design has zero tip mass. Substituting the changes in the beam lengths and the pedal length, (21), and the scaled tip mass \hat{R}_t in (14) for natural frequencies, the change in natural frequencies to first-order can be written as follows:

$$\omega_i^2 = (\omega_i^2)_c + \epsilon(S_{1i}\Delta v_2 + S_{2i}\Delta v_3 + S_{3i}\hat{R}_t), \quad i = 1, 2, \tag{22}$$

where

$$S_{1i} = \left(\frac{\partial \omega_i^2}{\partial v_2}\right)_c, \quad S_{2i} = \left(\frac{\partial \omega_i^2}{\partial v_3}\right)_c, \tag{23}$$

$$S_{21} = \left(\frac{\partial \omega_i^2}{\partial R_t}\right)_c, \quad i = 1, 2.$$

The parameters S_{1j} , S_{2j} , and S_{3j} define the sensitivities of the j 'th natural frequency to changes in the length of beam 2, length of the pedal, and the added mass at the tip of the pedal M_t , respectively. Note that the pedal mass is a function of the pedal length and as a result, the sensitivity S_{22} of the second natural frequency, ω_2 , with respect to the pedal length is not zero.

6.2 Resonance conditions

We are interested in studying the response of the microresonator for a resonant actuation of the in-plane flexural mode. The second mode can be resonantly excited when the frequency of AC voltage is near the

frequency of the second mode. Further, the microresonator is designed to have natural frequencies of the lowest torsional and flexural modes in 1:2 ratio. The internal resonance between the natural frequencies of the modes for nominal dimensions, denoted by $()_c$, and the resonant actuation are made explicit as follows:

$$(\omega_2)_c = 2(\omega_1)_c (1 + \epsilon\sigma_{in}), \tag{24}$$

$$\bar{\Omega} = (\omega_2)_c (1 + \epsilon\sigma_2),$$

where σ_{in} is a detuning between the torsional and the flexural modes from perfect 1:2 resonance, and σ_2 is the external detuning from perfect resonant actuation of the flexural mode. Using the resonance conditions in (24), the excitation frequency and the torsional natural frequency can be related as follows:

$$\bar{\Omega} = 2\omega_1(1 + \epsilon\sigma_1) + O(\epsilon^2), \tag{25}$$

where $\sigma_1 = \sigma_{in} + \sigma_2$.

6.3 Averaged equations

With equations properly scaled, we are in a position to now apply the method of averaging. For this, the scaled equations of motion (20) can be written in state-space form as follows:

$$\dot{\mathbf{u}} = \mathbf{A}\mathbf{u} + \epsilon \mathbf{w}(\mathbf{u}, \tau) + O(\epsilon^2), \tag{26}$$

where

$$\mathbf{u} = [u_{11}, u_{12}, u_{21}, u_{22}]^T,$$

$$u_{i1} = \hat{a}_i, \quad u_{i2} = \hat{a}_i, \quad i = 1, 2,$$

$$\mathbf{A} = \begin{bmatrix} 0 & 1 & 0 & 0 \\ -(\bar{\Omega}/2)^2 & 0 & 0 & 0 \\ 0 & 0 & 0 & 1 \\ 0 & 0 & -(\bar{\Omega})^2 & 0 \end{bmatrix}, \tag{27}$$

and

$$\mathbf{w} = \begin{bmatrix} 0 \\ -2\hat{\zeta}_1\omega_1 u_{12} + 2(\bar{\sigma}_{in} + \bar{\sigma}_2)\omega_1^2 u_{11} - 4\frac{\alpha}{R_1}\frac{\hat{G}_0}{R_1}\frac{h_0}{g_2}u_{21} - \frac{\alpha}{R_1}\omega_2^2 u_{11}u_{21} \\ 0 \\ \left(-2\hat{\zeta}_2\omega_2 u_{22} + 2\bar{\sigma}_2\omega_2^2 u_{21} + \frac{\alpha}{R_2}(u_{12}^2 - \omega_1^2 u_{11}^2 - \frac{\hat{G}_0}{R_1}\frac{h_0}{g_2}u_{11}) \right. \\ \left. + \frac{F}{R_2}(u_{22}^2 - 2\omega_2^2 u_{21}^2) + \frac{1}{R_2}(\hat{F}_1 \cos \bar{\Omega}\tau + \hat{F}_2 \cos 2\bar{\Omega}\tau) \frac{f_0}{g_1} \right) \end{bmatrix}, \tag{28}$$

with $\bar{\sigma}_{in}$ and $\bar{\sigma}_2$ defined as follows:

$$\begin{aligned} \bar{\sigma}_{in} = & \sigma_{in} + (1/2\omega_1^2) \left(\frac{\hat{G}_0 h_1}{R_1 g_2^2} - S_{11} \Delta v_2 - S_{21} \Delta v_3 \right. \\ & \left. - S_{31} \hat{R}_t \right) - (1/2\omega_2^2) \left(\frac{\hat{F}_0 f_1}{R_2 g_1^2} - 2\Gamma \frac{\hat{F}_0 f_0}{g_1 R_2^2} \right. \\ & \left. - S_{12} \Delta v_2 - S_{22} \Delta v_3 - S_{32} \hat{R}_t \right), \end{aligned} \tag{29}$$

$$\begin{aligned} \bar{\sigma}_2 = & \sigma_2 + (1/2\omega_2^2) \left(\frac{\hat{F}_0 f_1}{R_2 g_1^2} - 2\Gamma \frac{\hat{F}_0 f_0}{g_1 R_2^2} - S_{12} \Delta v_2 \right. \\ & \left. - S_{22} \Delta v_3 - S_{32} \hat{R}_t \right). \end{aligned}$$

The variable $\bar{\sigma}_{in}$ introduced above represents the effective mistuning of natural frequencies from 1:2 internal

resonance, and the variable $\bar{\sigma}_2$ represents the effective mistuning between the flexural mode natural frequency ω_2 and the excitation frequency $\bar{\Omega}$. The bias voltages related terms F_0 and G_0 in $\bar{\sigma}_1$ and $\bar{\sigma}_2$, respectively, capture the change in natural frequencies due to electrostatic forces. Note that the inertial nonlinearities due to in-plane rotation of the pedal about Z axis, terms with Γ , also result in mistuning the flexural mode natural frequency due to the nontrivial equilibrium position. The parameters ω_1 , ω_2 , R_1 , and R_2 in (28) and (29), and when used later in this section, are evaluated at the nominal dimensions (\cdot)_c.

The state space (26) are transformed into the standard form [10, 26] for applying the method of averaging using the following transformation:

$$\mathbf{u} = \Psi \mathbf{p}, \tag{30}$$

where

$$\Psi = \begin{bmatrix} \cos \frac{\bar{\Omega} \tau}{2} & \sin \frac{\bar{\Omega} \tau}{2} & 0 & 0 \\ -(\frac{\bar{\Omega}}{2}) \sin \frac{\bar{\Omega} \tau}{2} & (\frac{\bar{\Omega}}{2}) \cos \frac{\bar{\Omega} \tau}{2} & 0 & 0 \\ 0 & 0 & \cos \bar{\Omega} \tau & \sin \bar{\Omega} \tau \\ 0 & 0 & -(\bar{\Omega}) \sin \bar{\Omega} \tau & (\bar{\Omega}) \cos \bar{\Omega} \tau \end{bmatrix}, \tag{31}$$

and $\mathbf{p} = [p_1, q_1, p_2, q_2]^T$.

The transformation matrix Ψ is a fundamental matrix solution of the linear system given in (26). The transformed equations in standard form are:

$$\dot{\mathbf{p}} = \epsilon \Psi^{-1}(\tau) \mathbf{w}(\Psi \mathbf{p}, \tau) + O(\epsilon^2). \tag{32}$$

Using the standard form (32), first-order averaged equations for the original nonautonomous equations of motion, (13), are given by [10]:

$$\dot{\mathbf{p}} = \epsilon \frac{\bar{\Omega}}{4\pi} \int_0^{4\pi/\bar{\Omega}} \Psi^{-1}(\tau) \mathbf{w}(\Psi \mathbf{p}, \tau) d\tau. \tag{33}$$

The resulting averaged equations using (33) are:

$$\begin{aligned} \dot{p}_1 = & -\hat{\zeta}_1 \omega_1 p_1 - \bar{\sigma}_1 \omega_1 q_1 + \frac{\alpha}{R_1} \omega_1 (p_1 q_2 - q_1 p_2), \\ \dot{q}_1 = & -\hat{\zeta}_1 \omega_1 q_1 + \bar{\sigma}_1 \omega_1 p_1 - \frac{\alpha}{R_1} \omega_1 (p_1 p_2 + q_1 q_2), \\ \dot{p}_2 = & -\hat{\zeta}_2 \omega_2 p_2 - \bar{\sigma}_2 \omega_2 q_2 + \frac{1}{2} \frac{\alpha}{R_2} \omega_1 p_1 q_1, \end{aligned} \tag{34}$$

$$\begin{aligned} \dot{q}_2 = & -\hat{\zeta}_2 \omega_2 q_2 + \bar{\sigma}_2 \omega_2 p_2 - \frac{1}{4} \frac{\alpha}{R_2} \omega_1 (p_1^2 - q_1^2) \\ & + \frac{\hat{F}_1 f_0}{2R_2 \bar{\Omega} g_1}, \end{aligned}$$

where a dot now denotes derivative with respect to slow time $\epsilon \tau$. Thus, the variables (p_1, q_1) and (p_2, q_2) are slowly varying functions of time, and are asymptotic approximations to modal amplitudes a_1 and a_2 , respectively. Note that the equations for (p_1, q_1) and (p_2, q_2) are uncoupled linearly, and are only coupled through nonlinear quadratic terms.

The averaged equations (34) obtained here are of the same form as the averaged equations obtained for internally resonant oscillators coupled by quadratic nonlinearities and when excited externally in the higher frequency mode. The equilibrium solutions and stability analysis of the averaged system for such coupled oscillators has been conducted in detail by many researchers (see Chap. 2 in Nayfeh [7] for a quick overview). It has been shown that two types of equilibrium solutions arise: single-mode solutions

(with $p_1 = q_1 = 0$), and coupled-mode solutions (with all states nonzero). These solutions exist for different parameter combinations. The coupled-mode solution branches arise due to pitchfork bifurcation from single-mode solutions, and also exhibit turning points. The coupled-mode equilibrium responses can also undergo a Hopf bifurcation to limit cycle oscillations. Eventually, for some parameter combinations (and small damping), the limit cycles can lead to chaos by period-doubling bifurcations. These studies have been further extended to higher-order averaging analysis by Banerjee et al. [27], and a Melnikov analysis by Banerjee and Bajaj [28].

The analysis of averaged equations (34) for the case of resonant excitation of the flexural mode shows that there is a threshold voltage level (embedded in \hat{F}_1) below which the coupled-mode response does not arise, that is, the flexural mode cannot autoparametrically excite the torsional mode. This threshold actuation level is given by:

$$(\hat{F}_1)_{th} = \frac{2R_2\bar{\omega}g_1}{f_0} \left| \frac{R_1}{\alpha} \right| \omega_2 \sqrt{(\bar{\sigma}_1^2 + \hat{\zeta}_1^2)(\bar{\sigma}_2^2 + \hat{\zeta}_2^2)}, \tag{35}$$

and is the parameter combination needed for a pitchfork bifurcation from single-mode to coupled-mode solutions. Thus, for the flexural mode to autoparametrically excite the internally resonant torsional mode, the voltage level should be such that \hat{F}_1 is greater than the threshold forcing level given in (35). The significance of this threshold value will become apparent in the following section where results are more specifically presented and discussed. Note, however, that for zero dampings and mistunings, no threshold voltage is needed to excite the torsional mode.

7 Microresonator response and discussion

We now illustrate the performance of such a nonlinear microresonator by simulating the response of the pedal resonator configuration used as an example earlier in the linear analysis. Recall that the dimensions of the resonator are as given in (10). It was assumed that the resonator is made of polysilicon and a linear analysis resulted in specifying the pedal length of 102 μm , with specified beam dimensions, for 1:2 internal resonance between the lowest torsional and flexural modes. Thus, the dimensions in (10) along with the pedal length of

102 μm are the nominal dimensions of the resonator structure for having internal resonance.

Note the natural frequencies of the torsional and flexural modes, as predicted by linear analysis for nominal dimensions are not in perfect 1:2 resonance, and there is a small nonzero internal mistuning of $\sigma_{in} = -0.002/\epsilon$. Using the mode shapes obtained in linear analysis, the effective mistunings $\bar{\sigma}_{in}$ and $\bar{\sigma}_2$ for the resonator can be written as follows:

$$\begin{aligned} \bar{\sigma}_{in} &= (-2 \times 10^{-3} + 0.13 \times 10^{-3} V_{b2}^2 \\ &\quad - 0.6 \times 10^{-5} (V_{b1}^2 + 0.5 V_{ac}^2) / \epsilon \\ &\quad - 0.49 \Delta v_2 + 0.95 \Delta v_3 + 0.97 \hat{R}_t, \\ \bar{\sigma}_2 &= \sigma_2 + 0.6 \times 10^{-5} (V_{b1}^2 + 0.5 V_{ac}^2) / \epsilon \\ &\quad + 0.77 \Delta v_2 + 0.45 \Delta v_3 + 0.46 \hat{R}_t. \end{aligned} \tag{36}$$

This clearly shows that the effective internal mistuning $\bar{\sigma}_{in}$ between the natural frequencies from exact 1:2 internal resonance can be adjusted by varying the bias voltages, the beam lengths, as well as the attached mass particle.

Consider the resonator structure with nominal dimensions, and with no additional mass or length perturbations, that is $\hat{R}_t = \Delta v_2 = \Delta v_3 = 0$. Also, suppose that we set the bias voltage at electrode A, V_{b1} , to 10 Volts, a voltage which is much smaller than the static pull-in voltage of 158 Volts for electrode A; then the two linear modes about the deformed static equilibrium position of the pedal structure can be brought in near exact internal resonance ($\bar{\sigma}_{in} \simeq 0$) by appropriate choice of the bias voltage for the output electrode B. Thus, if we choose $V_{b2} = 4.46$ Volts, it results in decreasing the internal mistuning to $\bar{\sigma}_{in} = 0.6 \times 10^{-5} / \epsilon$ which clearly demonstrates the ability to change internal mistuning between the two modes by choice of bias voltages.

For the microresonator design proposed here, squeeze film damping is the most critical damping mechanism [29]. The damping can be reduced by operating the microresonator in vacuum. Designing the pedal with apertures can also reduce the damping significantly. Here, the damping for both the modes is assumed to be $\zeta_1 = \zeta_2 = 0.0001$ (corresponding to a quality factor $Q = 5,000$) except when the effect of damping on the response is considered.

7.1 A representative resonator response

Figures 9(a) and (b) show the simulated response amplitudes of the resonator using the averaged system (34) with bias voltages set to $V_{b1} = 10$ Volts and $V_{b2} = 4.46$ Volts. Figure 9(a) shows the out-of-plane (Z direction) displacement of the resonator at the pedal tip point D (Z_D), see Fig. 1, as a function of the actuation signal frequency for different values of the applied AC voltage signal, V_{ac} . Figure 9(b) shows the corresponding in-plane (Y direction) displacement at the pedal point C (Y_C). The figures show that the structure responds linearly and moves only in the transverse direction until a threshold AC voltage level of $V_{ac} \simeq 0.005$ Volts is achieved. However, when the threshold voltage is exceeded, the in-plane flexural motion becomes unstable (indicated by dotted lines) and a new stable response arises due to pitchfork bifurcation, as is clearly indicated in Fig. 9(a) for the torsional response. In this stable response, the nonlinear interaction between the flexural mode and the torsional mode results in an out-of-plane rotation of the pedal at half the input frequency due to the participation of the torsional mode in the response. Thus, the out-of-plane response will be zero unless the torsional mode participates. As can be seen, the indirectly excited mode

responds only in a small frequency interval around the directly excited resonant frequency. Furthermore, the frequency bandwidth over which the pedal responds with out-of-plane displacement can be controlled by changing the actuation level.

The uniqueness of the present resonator response is in the actuation of an out-of-plane mode (torsional) through resonant actuation of an in-plane lateral mode (flexural). Further, the out-of-plane response is completely different from the response of a typical linear microresonator in three ways: (1) the out-of-plane response is nonzero only for a narrow bandwidth of input signal frequency centered about the natural frequency of the lateral mode, (2) the out-of-plane response is at half the input signal frequency, and (3) the bandwidth can be controlled by varying voltage signal. Thus, if the pedal motion is measured electrostatically through electrode B or by out-of-plane vibrometer, it will result in capturing the unique nonlinear response of the microresonator. From an applications perspective, these characteristics make the resonator suitable for RF MEMS filtering and mixing device with exceptional rejection for stop band rejection characteristics. It is also interesting to note that in the bandwidth of operation where the out-of-plane response is nontrivial, the response amplitude remains relatively constant

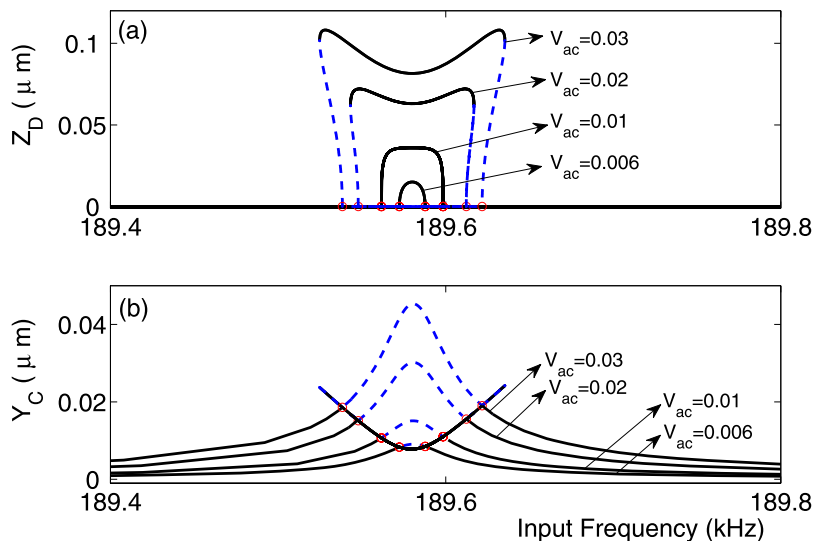


Fig. 9 Response of a pedal microresonator when excited resonantly in the in-plane flexural mode as a function of input frequency for different actuation voltages (V_{ac} in Volts). (a) The out-of-plane displacement at the tip of the pedal (Z_D); (b) In-plane displacement of the pedal (Y_C). Parameters of the mi-

croresonator are: $L_1 = L_2 = 100 \mu\text{m}$, $L_p = 102 \mu\text{m}$, $t = 3 \mu\text{m}$, $b = 5 \mu\text{m}$, $b_p = 25 \mu\text{m}$, $d_1 = d_2 = 2 \mu\text{m}$, $V_{b1} = 10$ Volts, $V_{b2} = 4.46$ Volts, $\zeta_1 = \zeta_2 = 0.0001$, $E = 170$ GPa, $\rho = 2330 \text{ kg/m}^3$, $\nu = 0.22$. *Solid lines* represent stable response and *dotted lines* represent unstable response

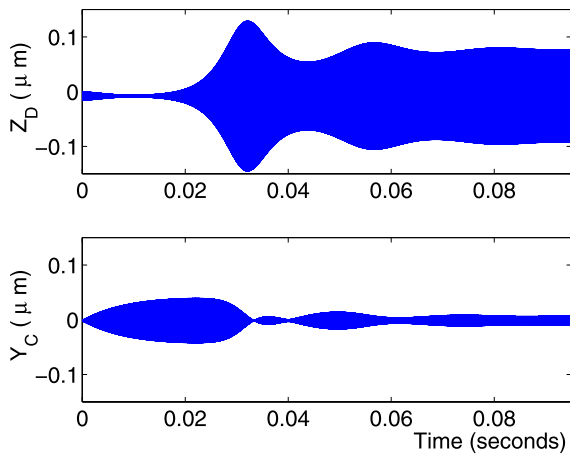


Fig. 10 The microresonator response as a function of time using direct numerical integration of two-mode reduced-order model for actuation voltage $V_{ac} = 0.03$ Volts and actuation frequency $\Omega = 189.581$ kHz. (a) The out-of-plane displacement at the tip of the pedal (Z_D); (b) In-plane displacement of the pedal (Y_C). Parameters of the microresonator are: $L_1 = L_2 = 100 \mu\text{m}$, $L_p = 102 \mu\text{m}$, $t = 3 \mu\text{m}$, $b = 5 \mu\text{m}$, $b_p = 25 \mu\text{m}$, $d_1 = d_2 = 2 \mu\text{m}$, $V_{b1} = 10$ Volts, $V_{b2} = 4.46$ Volts, $\zeta_1 = \zeta_2 = 0.0001$, $E = 170$ GPa, $\rho = 2330$ kg/m³, $\nu = 0.22$

over the whole frequency interval. This is distinct from the resonantly excited linear MEMS resonators where the response rolls off rather sharply away from exact resonance.

In Fig. 10, the time responses of the resonator are shown in terms of the displacements Y_C and Z_D at a given actuation frequency $\Omega = 189.581$ kHz and AC voltage $V_{ac} = 0.03$ Volts. These were obtained by a direct numerical integration of the two-mode reduced order model in (13). Note that the actuation signal frequency corresponds to $\bar{\sigma}_2 = 0$, that is, the natural frequency of the flexural mode (mistuned by bias voltage V_{b2}) is in perfect resonance with the actuation signal frequency. The simulation here was started with zero initial conditions for velocities and displacements of both the modal amplitudes, and the electrostatic nonlinearities up to fifth-order were retained in the model. The steady-state amplitude is reached in about 0.080 secs, and the steady-state amplitudes for transverse displacement (Y_C) and out-of-plane displacement at tip D (Z_D) are 8.2 nm (with mean deflection ~ -1.6 nm) and 0.086 μm (with mean deflection ~ -8.9 nm), respectively. The corresponding amplitudes from averaged system response in Fig. 9 are $Y_C = 7.8$ nm and $Z_B = 0.082 \mu\text{m}$. Thus, the original system response matches very well with the pre-

dictions of the asymptotic analysis through averaged equations. Also, the mean deflections of the pedal point C and the pedal tip D are close to the approximate static deflections predicted by (17).

7.2 Effect of damping

Damping plays a very crucial role in the resonator response. The effect of damping in general on the response of two degree of freedom autoparametric systems is detailed in [7, 10]. Furthermore, for a given excitation voltage V_{ac} , a decrease in damping in the first and second modes along with mistuning from 1:2 internal resonance can result in a Hopf bifurcation in the response. This can be further accompanied by period doubling bifurcations and chaotic motions of the beam at higher excitation or lower damping levels [10]. As already pointed out, the threshold actuation level, (35), needed for coupled-mode response essential to the performance of the present resonator is strongly dependent on the system damping.

Figure 11 illustrates the response of the resonator for higher modal dampings, with ζ_1 and ζ_2 set to 0.001. These damping values correspond to a quality factor of 500 for each of the modes, and can be achieved for microresonators operating in air [30]. The bias voltages and other parameters, except for dampings, remain unchanged from the parameters used for Fig. 9. Since both the dampings are increased tenfold, the threshold voltage increases hundred times to $V_{ac} \simeq 0.5$ Volts. Thus, the minimum voltage required to indirectly excite the torsional mode increases as the damping increases.

7.3 Effects of length variations

As introduced earlier, the natural frequencies for the two interacting modes are sensitive to variations in length of the beams as well as the pedal. First, we study the effect of variations in the beam lengths on the response of the example pedal microresonator. This variation in beam lengths significantly affects the mistunings $\bar{\sigma}_2$ and $\bar{\sigma}_{in}$, as expressed through the formulas in (36). This in turn affects the threshold voltage (see (35)) needed for the coupled-mode response to arise, and hence the torsional mode to be activated. Figure 12 shows the response of the system for three different lengths L_2 of the beam 2, $L_2 = 100.01$, 100.1, and 101 μm . The mistunings in

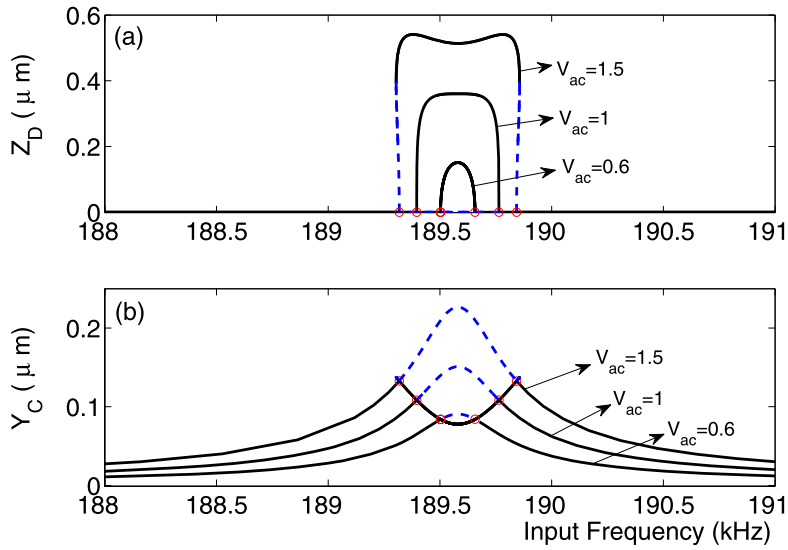


Fig. 11 Response of the pedal microresonator for increased dampings $\zeta_1 = \zeta_2 = 0.001$ as a function of input frequency for different actuation voltages (V_{ac} in Volts). **(a)** The out-of-plane displacement at the tip of the pedal (Z_D); **(b)** In-plane displacement of the pedal (Y_C). Parameters of the microresonator

are: $L_1 = L_2 = 100 \mu\text{m}$, $L_p = 102 \mu\text{m}$, $t = 3 \mu\text{m}$, $b = 5 \mu\text{m}$, $b_p = 25 \mu\text{m}$, $d_1 = d_2 = 2 \mu\text{m}$, $V_{b1} = 10$ Volts, $V_{b2} = 4.46$ Volts, $E = 170$ GPa, $\rho = 2330$ kg/m³, $\nu = 0.22$. Solid lines represent stable response and dotted lines represent unstable response

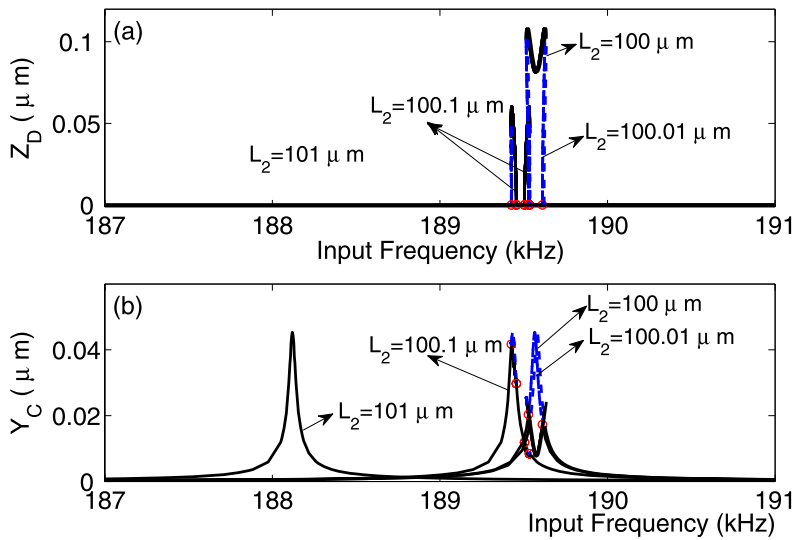


Fig. 12 Response of the pedal microresonator for different lengths of beam 2, $L_2 = 101 \mu\text{m}$, $100.1 \mu\text{m}$, and $100.01 \mu\text{m}$, as a function of input frequency. The actuation AC voltage is fixed at $V_{ac} = 0.03$ Volts. **(a)** The out-of-plane displacement at the tip of the pedal (Z_D); **(b)** In-plane displacement of the

pedal (Y_C). Parameters of the microresonator are: $L_1 = 100 \mu\text{m}$, $L_p = 102 \mu\text{m}$, $t = 3 \mu\text{m}$, $b = 5 \mu\text{m}$, $b_p = 25 \mu\text{m}$, $d_1 = d_2 = 2 \mu\text{m}$, $V_{b1} = 10$ Volts, $V_{b2} = 4.46$ Volts, $\zeta_1 = \zeta_2 = 0.0001$, $E = 170$ GPa, $\rho = 2330$ kg/m³, $\nu = 0.22$. Solid lines represent stable response and dotted lines represent unstable response

the slow evolution equations due to these variations in the length of beam 2 were calculated using (36) with Δv_2 defined using (21). All the parameters ex-

cept length L_2 remain unchanged from the parameters used for Fig. 9. The AC voltage level is set to $V_{ac} = 0.03$ Volts.

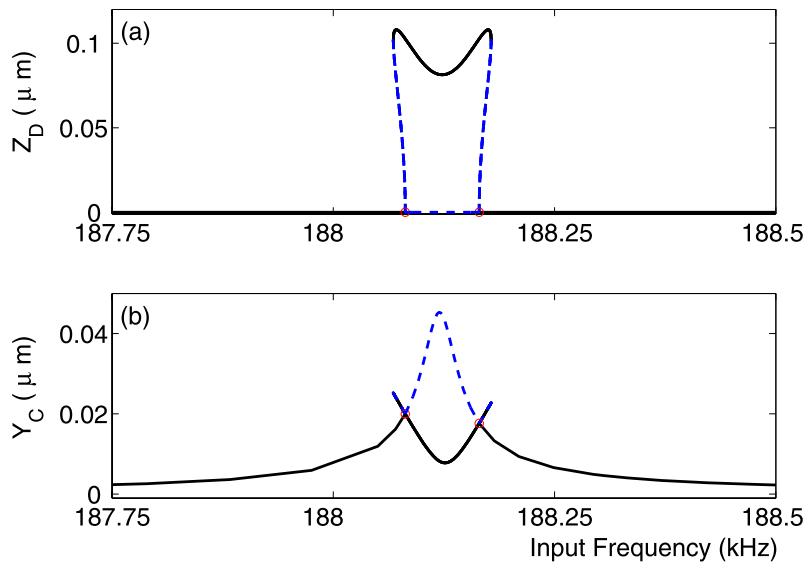


Fig. 13 Response of the microresonator with electrode B bias voltage adjusted to $V_{b2} = 7.51$ Volts to remove the internal mistuning resulting from change in the length of beam 2 with $\Delta\nu_2 = 0.01$. The actuation AC voltage is fixed at $V_{ac} = 0.03$ Volts. **(a)** The out-of-plane displacement at the tip of the

pedal (Z_D); **(b)** In-plane displacement of the pedal (Y_C). Parameters of the microresonator are: $L_1 = 100 \mu\text{m}$, $L_2 = 101 \mu\text{m}$, $L_p = 102 \mu\text{m}$, $t = 3 \mu\text{m}$, $b = 5 \mu\text{m}$, $b_p = 25 \mu\text{m}$, $d_1 = d_2 = 2 \mu\text{m}$, $V_{b1} = 10$ Volts, $\zeta_1 = \zeta_2 = 0.0001$, $E = 170$ GPa, $\rho = 2330 \text{ kg/m}^3$, $\nu = 0.22$

As can be seen from Fig. 12(b), variation in the length of beam 2 changes the natural frequency of the flexural mode. However, Fig. 12(a) shows that the out-of-plane response of the pedal is affected more drastically, and determines through internal mistuning $\bar{\sigma}_{in}$ whether or not the torsional mode can be indirectly excited. For $L_2 = 101 \mu\text{m}$, the internal mistuning is large enough that the torsional mode is not excited. Thus, the pedal moves only in Y-direction in the XY plane. As demonstrated below, the pedal response in the torsional or out-of-plane mode can be reactivated by tuning the natural frequencies nearer to 1:2 resonance, by increasing the actuation level, or by reducing the resonator modal dampings.

Here, we discuss the use of bias voltages in tuning natural frequencies as a means to counteract variation in the length of beam 2. As mentioned earlier, the effective internal mistuning $\bar{\sigma}_{in}$, (36), depends on bias voltages as well as on the variation in lengths and on added mass. For $L_2 = 101 \mu\text{m}$, natural frequencies of the modes can be tuned to 1:2 internal resonance by increasing bias voltage at electrode B, V_{b2} , to 7.51 Volts while keeping the bias voltage at electrode A at the same value of 10 Volts. The response of the resonator with bias voltage $V_{b2} = 7.51$ Volts

and length of beam 2 at $L_2 = 101 \mu\text{m}$ is shown in Fig. 13. Also, note that the effective internal mistuning between the natural frequencies for zero bias voltages is -0.69% for $\epsilon = 1$.

Unequal beam lengths also implies that the slope of the beams at the pedal end can be nonzero, and as a result the pedal can rotate about Z-axis in the XY plane. Since the mode shapes used in obtaining the effective mistunings, (36), are for a resonator configuration with equal beam lengths, the effect of pedal rotation in XY plane is not captured by the mistunings. To see the effect of the rotation of pedal in XY plane, we obtain linear mode shapes for a pedal resonator with a different length of beam 2, $L_2 = 101 \mu\text{m}$, while keeping all other parameters the same. The resulting natural frequencies of the torsional and the flexural modes for zero bias voltages are mistuned by -0.70% from 1:2 internal resonance ($\bar{\sigma}_{in} = -0.0070$ for $\epsilon = 1$). Thus, for a length variation corresponding to a nondimensional variable $\Delta\nu_2 = 0.01$, the effect of including the pedal rotation about Z-axis is not significant.

The coefficients of parameter for change in pedal length $\Delta\nu_3$, see (36), that define the change in natural frequencies are different from those for parameter $\Delta\nu_2$. Thus, the effect of variation in pedal length

differs only in sensitivity from the effect of variation in beam 2 length. Equating the sensitivities for $\Delta\nu_2$ and $\Delta\nu_3$ in the equation for $\bar{\sigma}_{in}$, we can conclude for the present example that the effect of having beam 2 lengths of 101 μm , 101.1 μm , and 101.01 μm on internal mistuning, and consequently, indirect excitation of the torsional mode, is equivalent to having pedal lengths of approximately 102.5 μm , 102.95 μm , and 102.995 μm , respectively. Thus, the frequency mistunings are twice as sensitive to the changes in the pedal length as compared to the changes in the length of beam 2.

7.4 Effect of adding a tip mass

Sensitivity of natural frequencies to placement of a mass particle on the pedal tip is captured by the coefficient of \hat{R}_t in (36). Placing a mass particle on the resonator can be a functional requirement if the resonator is used as a mass sensor device, or commercially available mass particles can be used as a tool for tuning the resonator to 1:2 internal resonance following fabrication.

The shift in natural frequencies due to the addition of mass depends on sensitivities S_{3j} , $j = 1, 2$, and the ratio R_t of the mass of the added particle to the mass of the pedal structure. Thus, as expected, a smaller sized structure will result in a larger shift in frequency for the same mass particle. This shift in natural frequencies results in mistuning the resonator from 1:2 internal resonance. The indirectly excited out-of-plane motion of the pedal is very sensitive to any internal resonance mistunings, and this sensitivity of the indirectly excited response can be utilized in making a mass sensor device based on the nonlinear pedal microresonator.

Figure 14 shows the effect of adding a particle of mass $\sim 6 \times 10^{-12}$ gm (or 6 pgm) on the pedal tip which corresponds to $R_t = 0.0002$. Except for the AC voltage and the added mass, all other parameters are the same as used for Fig. 9. There are three responses shown: (i) no mass on the pedal and AC voltage set to $V_{ac} = 0.01$ Volts, (ii) a mass of 6 pgm added to the pedal tip, and the voltage kept the same at $V_{ac} = 0.01$ Volts, and (iii) a mass of 6 pgm attached to the pedal tip, and the voltage level increased by

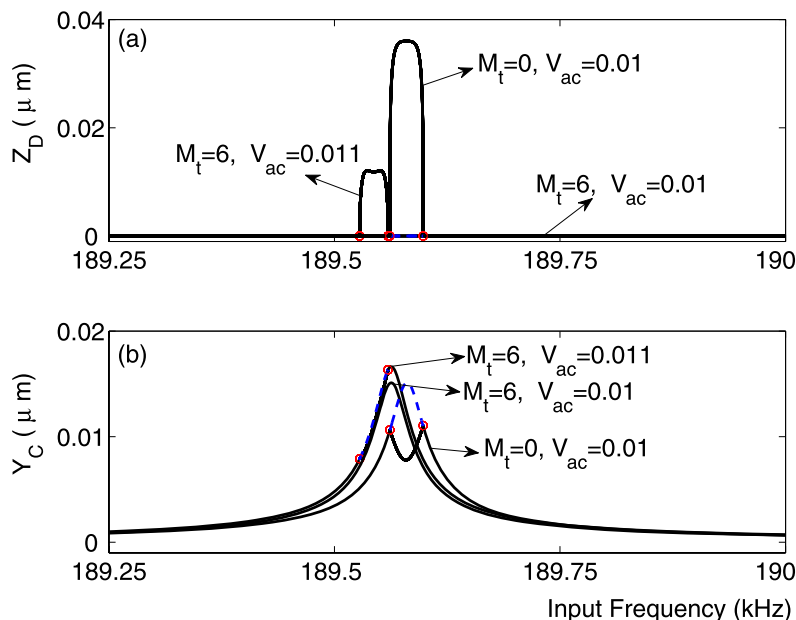


Fig. 14 Response of the microresonator as a function of input AC signal frequency for: (i) zero added mass and AC voltage $V_{ac} = 0.01$ Volts, (ii) an added mass of 6 picogm at the pedal tip D and $V_{ac} = 0.01$ Volts, and (iii) an added mass of 6 picogm at the pedal tip D with $V_{ac} = 0.011$ Volts. (a) The out-of-plane

displacement at the tip of the pedal (Z_D); (b) In-plane displacement of the pedal (Y_C). Parameters of the microresonator are: $L_1 = L_2 = 100 \mu\text{m}$, $L_p = 102 \mu\text{m}$, $t = 3 \mu\text{m}$, $b = 5 \mu\text{m}$, $b_p = 25 \mu\text{m}$, $d_1 = d_2 = 2 \mu\text{m}$, $V_{b1} = 10$ Volts, $V_{b1} = 4.46$ Volts, $\zeta_1 = \zeta_2 = 0.0001$, $E = 170$ GPa, $\rho = 2330$ kg/m³, $\nu = 0.22$

1 mV to $V_{ac} = 0.011$ Volts. In case (i), the pedal tip point D oscillates in an out-of-plane motion with amplitude of $\sim 0.04 \mu\text{m}$ when the AC signal frequency is in resonance with the flexural mode natural frequency. When a mass of 6 pgm is attached to the pedal tip while keeping the same actuation level, case (ii), the torsional mode is sufficiently mistuned away from exact internal resonance, and, therefore, it is not excited. As a result, the pedal moves only in Y direction in the XY plane and no response is measured on electrode B. If, however, when the voltage level is now increased to $V_{ac} = 0.011$ Volts, case (iii), the pedal again moves in the out-of-plane Z direction with amplitude of response smaller than the amplitude for zero added mass and $V_{ac} = 0.01$ Volts. Thus, the response of the pedal in the indirectly excited mode is very sensitive to added mass and can switch from nonzero to zero amplitude due to the addition of a small mass. Linear microresonators have been designed that utilize a shift in natural frequency to detect addition of mass [2, 31]; for the present nonlinear pedal microresonator, a shift in actuation level required to reactivate the out-of-plane motion of the pedal can be used to detect presence of additional mass.

8 Summary and conclusion

A pedal microresonator operating on the principle of nonlinear modal interactions arising due to autoparametric 1:2 resonance between the lowest torsional and flexural modes of the resonator is introduced in this study. Nominal dimensions of the resonator, for having the lowest torsional and flexural mode frequencies in 1:2 ratio, are determined using linear analysis. The flexural mode results in an in-plane motion of the pedal, while the torsional mode results in an out-of-plane motion of the pedal. For analyzing the resonator response for electrostatic actuation of the flexural mode through a lateral electrode, a two-mode reduced-order model is developed using the torsional and flexural mode shapes. The reduced-order model retains quadratic nonlinearities coupling the flexural and torsional modes. Asymptotic equations obtained by first-order averaging are used to determine the response of an example pedal microresonator.

A typical response of such a resonator shows four unique characteristics in comparison to a linear microresonator: (1) laterally actuated in-plane flexural

mode results in exciting the internally resonant torsional mode through autoparametric 1:2 resonance, (2) the out-of-plane response of the pedal structure arising due to the participation of torsional mode is nonzero only for an actuation signal frequency interval around the natural frequency of the directly excited flexural mode, (3) the frequency bandwidth over which the torsional mode participates, and sets the pedal in out-of-plane motion, can be controlled by actuation voltage, and (4) out-of-plane response of the pedal is at half the frequency of the actuation signal. Because of these unique characteristics, the nonlinear microresonator design holds great potential for use in RF mixer-filter and sensor devices.

The operation of such a resonator is very sensitive to any mistuning in 1:2 resonance between the modes. Adding a mass particle on the resonator impacts drastically the participation of the indirectly excited torsional mode in the resonator response. For a very small mass perturbation, the out-of-plane response of the pedal can switch from nonzero (torsional mode participating) to zero amplitude (torsional mode not participating). However, the torsional mode can be reactivated by increasing the actuation level. The required increase in the actuation level can transduce the addition of mass, and thereby the microresonator can also be used as a mass sensor.

We finally note that this work is part of a much larger dedicated effort on design and development of nonlinear responses based MEMS resonators. The authors are currently working on fabricating such 1:2 internal resonance based microresonators and experimentally verifying the performance characteristics observed in the analytical results.

References

1. Zhnag, W., Turner, K.L.: Application of parametric resonance amplification in a single-crystal silicon micro-oscillator based mass sensor. *Sens. Actuators A* **122**, 23–30 (2005)
2. Gupta, A., Akin, D., Bashir, R.: Single virus particle mass detection using microresonators with nanoscale thickness. *Appl. Phys. Lett.* **84**(11), 1976–1978 (2004)
3. Nguyen, C.T.-C.: Vibrating RF MEMS for next generation wireless applications. In: *Proceedings of the Custom Integrated Circuits Conference*, Orlando, FL, 3–6 October. IEEE, Piscataway (2004)
4. Rutzel, S., Lee, S.I., Raman, A.: Nonlinear dynamics of atomic-force-microscope probes driven in Lennard-Jones potential. *Proc. R. Soc. Lond.* **459**, 1925–1948 (2003)

5. Younis, M.I., Nayfeh, A.H.: A study of the nonlinear response of a resonant microbeam to an electric actuation. *Nonlinear Dyn.* **31**, 91–117 (2003)
6. Turner, K.L., Miller, S.A., Hartwell, P.G., MacDonald, N.C., Strogatz, S.H., Adams, S.G.: Five parametric resonances in a microelectromechanical system. *Nature* **396**(6707), 149–152 (1998)
7. Nayfeh, A.H.: *Nonlinear Interactions: Analytical, Computational and Experimental Methods*. Wiley-Interscience, New York (2000)
8. Balachandran, B., Nayfeh, A.H.: Nonlinear motions of a beam-mass structure. *Nonlinear Dyn.* **1**, 39–61 (1990)
9. Haxton, R.S., Barr, A.D.S.: The autoparametric vibration absorber. *ASME J. Eng. Ind.* **94**, 119–225 (1972)
10. Bajaj, A.K., Chang, S.I., Johnson, J.: Amplitude modulated dynamics of a resonantly excited autoparametric two degree-of-freedom system. *Nonlinear Dyn.* **5**, 433–457 (1994)
11. Vyas, A., Bajaj, A.K.: Microresonators based on 1:2 internal resonance. In: *Proceedings of IMECE'05*, Orlando, FL, 5–11 November. ASME Paper No. IMECE2005-61955 (2005)
12. Baskaran, R., Turner, K.L.: Mechanical domain coupled mode parametric resonance and amplification in a torsional mode micro electro mechanical oscillator. *J. Micromech. Microeng.* **13**, 701–707 (2003)
13. Nayfeh, A.H., Mook, D.T.: *Nonlinear Oscillations*. Wiley-Interscience, New York (1979)
14. Carr, D.W., Evoy, S., Sekaric, L., Craighead, H.G.: Parametric amplification in a torsional microresonator. *Appl. Phys. Lett.* **77**(10), 1545–1547 (2000)
15. Zhang, W., Baskaran, R., Turner, K.: Tuning the dynamic behavior of parametric resonance in a micromechanical oscillator. *Appl. Phys. Lett.* **82**(1), 130–132 (2003)
16. Zalalutdinov, M., Olkhovets, A., Zehnder, A., Ilic, B., Czapslewski, D., Craighead, H.G., Parpia, J.M.: Optically pumped parametric amplification for micromechanical oscillators. *Appl. Phys. Lett.* **78**(20), 3142–3144 (2001)
17. Nayfeh, A.H., Pai, P.F.: *Linear and Nonlinear Structural Mechanics*. Wiley-Interscience, New York (2002)
18. Young, W.C.: *Roark's Formulas for Stress & Strain*. McGraw-Hill, New York (1989)
19. Crespo Da Silva, M.R.M.: Nonlinear flexural-flexural-torsional-extensional dynamics of beams, I: formulation. *Int. J. Solids Struct.* **24**, 1225–1234 (1988)
20. Crespo Da Silva, M.R.M., Zaretzky, C.L.: Nonlinear flexural-flexural-torsional interactions in beams including the effect of torsional dynamics, I: primary resonance. *Nonlinear Dyn.* **5**, 3–23 (1994)
21. Sharpe, W.N. Jr., Yuan, B., Vaidyanathan, R., Edwards, R.L.: Measurements of Young's modulus, Poisson's ratio, and tensile strength of polysilicon. In: *Proceedings of the IEEE Micro Electro Mechanical Systems*, Nagoya, Japan, pp. 424–429. IEEE, Piscataway (1997)
22. Degani, O., Lipson, A., Leitner, T., Setter, D.J., Kaldor, S., Nemirovsky, Y.: Pull-in study of an electrostatic torsion microactuator. *J. Microelectromech. Syst.* **7**, 373–379 (1998)
23. Pamidighantam, S., Puers, R., Baert, K., Tilmans, H.A.C.: Pull-in voltage analysis of electrostatically actuated beam structures with fixed-fixed and fixed-free end conditions. *J. Micromech. Microeng.* **12**, 458–464 (2002)
24. Daqaq, M.F.: *Adaptation of nontraditional control techniques to nonlinear micro and macro mechanical systems*. PhD thesis, Virginia Polytechnic Institute and State University, Blacksburg, VA (2006)
25. Daqaq, M.F., Abdel-Rahman, E.M., Nayfeh, A.H.: Modal interactions in resonant microscanners. In: *Proceedings of IMECE'06*, Chicago, 5–10 November. ASME Paper No. IMECE2006-13844 (2006)
26. Murdock, J.A.: *Perturbations: Theory and Methods*. Wiley, New York (1991)
27. Banerjee, B., Bajaj, A.K., Davies, P.: Resonant dynamics of an autoparametric system: a study using higher-order averaging. *Int. J. Non-Linear Mech.* **31**, 21–39 (1996)
28. Banerjee, B., Bajaj, A.K.: Amplitude modulated chaos in two degree-of-freedom systems with quadratic nonlinearities. *Acta Mech.* **124**, 131–154 (1997)
29. Corman, T., Enoksson, P., Stemme, G.: Gas damping of electrostatically excited resonators. *Sens. Actuators A: Phys.* **61**, 249–255 (1997)
30. Tilmans, H.A.C., Raedt, W.D., Beyne, E.: MEMS for wireless communications: 'from RF-MEMS components to RF-MEMS-SiP'. *J. Micromech. Microeng.* **13**, S139–S163 (2003)
31. Ilic, B., Czapslewski, D., Craighead, H.G.: Mechanical resonant immunospecific biological detector. *Appl. Phys. Lett.* **77**(3), 450–452 (2000)